NASA Technical Paper 3077

May 1991

Span Reduction Effects on Flutter Characteristics of Arrow-Wing Supersonic Transport Configurations

Donald F. Keller
and Ellen Parker Bullock

NASA

NASA Technical Paper 3077

1991

Span Reduction Effects on Flutter Characteristics of Arrow-Wing Supersonic Transport Configurations

Donald F. Keller and Ellen Parker Bullock
Langley Research Center
Hampton, Virginia

NASA
National Aeronautics and Space Administration
Office of Management
Scientific and Technical Information Division

Summary

An experimental and analytical investigation was initiated to determine the effects of span reduction on the flutter characteristics of several arrow-wing supersonic transport (SST) configurations. The model was a semispan wing with a 3-percent biconvex airfoil. The wing leading-edge sweep was 73° for the inboard 70 percent of the span and 60° for the outboard 30 percent of the span. Two flow-through nacelles were used to represent wing-mounted engines. A wing fin with a 3-percent biconvex airfoil was mounted either vertically or canted outboard at 45°. Portions of the wingtip were removed in increments parallel to the root chord to provide reductions in wing span of 10, 20, and 30 percent.

Experimental flutter results were obtained in the Langley Transonic Dynamics Tunnel (TDT) over a Mach number range from 0.60 to 1.20 with a heavy gas (R-12) as the test medium. All test configurations had a similar flutter behavior and no unusual flutter mechanisms were encountered. Flutter points in the low transonic region were dominated by the wing first-torsion mode and involved considerable midwing, leading-edge deflections. The high transonic flutter points were dominated by the wing first-bending mode and were characterized by large wingtip deflections. Reducing the wingspan increased the flutter dynamic pressure boundaries for all configurations tested. The largest increases in the flutter dynamic pressure boundaries were observed for the configurations with nacelles. Although reducing the span had little effect on the flutter-speed index boundaries for the wing only and wing with fin configurations, an increase was observed for the configurations with nacelles, particularly in the high transonic region.

Analytical flutter results are compared with experimental flutter results over a Mach number range from 0.60 to 0.95 for the wing only and the wing with nacelles configurations. Analytical results were calculated for each reduction in span with unsteady aerodynamic subsonic kernel function theory. In general, the analytical flutter boundaries showed the same trends as the experimental flutter boundaries, although the analysis was consistently more conservative in the low transonic region than in the high transonic region.

Introduction

Long-range international air travel has increased significantly in recent years and is projected to continue to increase well into the 21st century (ref. 1). This increase in long-range air travel along with advances in flight technologies, such as aircraft structures, materials, propulsion, and electronics, has resulted in a renewed interest in supersonic cruise aircraft. The High Speed Civil Transport (HSCT) and the National Aero-Space Plane (NASP) are two examples of current supersonic cruise research programs.

During the Supersonic Transport (SST) Program of the 1960's and the subsequent research programs of the 1970's and early 1980's, a number of major technical problems were identified (ref. 2). Among these were documented flutter deficiencies in strength-designed supersonic cruise aircraft. Because these aircraft were generally large and flexible structures, additional stiffness was necessary to satisfy flutter clearance requirements. This usually results in an increase in structural weight or a redesign of critical structural components (refs. 3 through 8). Additional weight degrades aircraft performance and increases costs. A control system synthesis and evaluation performed on an arrow-wing supersonic cruise configuration indicated that the implementation of a flutter suppression system could also increase the flutter speed without degrading aircraft reliability and performance (ref. 9). Additionally, an active flutter suppression control system has been demonstrated successfully in a wind-tunnel test conducted on a simplified version of a supersonic transport wing (ref. 10). Such a system, however, has not been tested on a full-scale transport aircraft.

In the 1960's NASA developed an SST configuration during its Supersonic Cruise Air Transport (SCAT) Studies which offered aerodynamic performance well above other previous designs (refs. 2 and 11). An arrow-wing planform was chosen for this design (SCAT-15F) because of its compromise between subsonic (moderately swept outboard portion of the wing) and supersonic (highly swept inboard portion of the wing) performance. In fact, many current HSCT concepts being developed by major airframe manufacturers employ arrow-wing planforms (ref. 1). However, as with other supersonic cruise transport designs, flutter is an important design consideration in the development of an arrow-wing configuration. Some earlier studies of full span models (refs. 4, 12, and 13) and of more simple small-scale, semispan arrow wings (refs. 14, 15, and 16) are presented in the literature. These studies, which included the addition of engine nacelles mounted on the wing lower surface and/or a fin mounted on the wing upper surface, showed that arrow-wing HSCT configurations could have difficulty meeting flutter-speed requirements in the transonic region.

The present study was undertaken to investigate the extent that reducing the span of the outboard lower swept region of the wing would affect the flutter characteristics of several arrow-wing configurations and to increase the available flutter data base for arrow-wing designs. Results from analytical and experimental studies exploring the effect of span variation on the flutter characteristics of highly swept wing configurations are presented in references 3 and 17, respectively. The semispan arrow-wing model used in this study was based on a Langley Advanced Supersonic Technology (AST-200) series design (ref. 18). This arrow-wing design was a refinement of an earlier Supersonic Cruise Aircraft Research (SCAR) transport concept designed for a cruise Mach number of 2.7 (ref. 3). The experimental transonic flutter boundaries presented in this paper were obtained from wind-tunnel tests conducted with the model at an angle of attack of 0°.

A flutter analysis was performed with a subsonic kernel function flutter prediction program. The purpose of the analysis was to evaluate the program's ability to predict arrow-wing flutter phenomenon and to provide a better understanding of arrow-wing flutter characteristics. The results of this analysis are compared with the flutter results from the wind-tunnel test.

Symbols

AR	panel aspect ratio
b	reference length, mean aerodynamic semichord, ft
c.g.	center of gravity
f	frequency, Hz
f_a	analytical (calculated) natural frequency, Hz
f_f	flutter frequency, Hz
f_f/f_2	flutter frequency ratio
f_m	measured natural frequency, Hz
f_2	reference frequency, Hz
H	total pressure, psf
I_{XX}	roll inertia about wing c.g., slug-ft^2
I_{YY}	pitch inertia about wing c.g., slug-ft^2
I_{ZZ}	yaw inertia about wing c.g., slug-ft^2
$I_{XX,e}$	roll inertia about engine nacelle c.g., slug-ft^2
$I_{YY,e}$	pitch inertia about engine nacelle c.g., slug-ft^2
$I_{ZZ,e}$	yaw inertia about engine nacelle c.g., slug-ft^2
$I_{XX,f}$	roll inertia about fin c.g., slug-ft^2
$I_{YY,f}$	pitch inertia about fin c.g., slug-ft^2
$I_{ZZ,f}$	yaw inertia about fin c.g., slug-ft^2
M	Mach number
m_o	total wing mass (minus mass of two mounting tabs), slugs
q	dynamic pressure, psf
Re	Reynolds number per foot
S	planform area, in^2
v_r	reference volume (conical frustum surrounding wing model), ft^3
V_f	flutter velocity, ft/sec
V_I	flutter-speed index, $\frac{V_f}{\omega_2 b(\mu^{1/2})}$
x	streamwise coordinate (positive downstream), in.
y	spanwise coordinate (positive outboard), in.
z	vertical coordinate (positive up), in.
μ	mass ratio, $m_o/\rho v_r$
ρ	density, slugs/ft^3
ω_2	$= 2\pi f_2$, rad/sec

Test Apparatus

Wind Tunnel

The test was conducted in the Langley Transonic Dynamics Tunnel (TDT). (See ref. 19.) The TDT is a continuous-flow, single-return, slotted-throat wind tunnel. The test section is 16 ft by 16 ft square with cropped corners. The tunnel is equipped to operate with air or a heavy gas (R-12) as the test medium. R-12 was used exclusively in the present study. Tunnel speed and stagnation pressure are independently controllable from Mach numbers of near 0 to 1.2 at pressures ranging from near 0 to 1 atmosphere. The TDT operating envelope, with R-12 as the test medium, is shown in figure 1. Also, the TDT is equipped with quick-opening bypass valves which can be activated to rapidly reduce test-section Mach number and dynamic pressure when flutter occurs to minimize the risk of model damage.

These capabilities make the TDT ideally suited for flutter testing.

Model and Components

The generic semispan cantilevered arrow-wing model used in this study was designed to represent a 1/20th-scale AST-200 series arrow-wing SST. A photograph of the model mounted in the TDT is presented in figure 2. The planform shape and dimensions of the wing are presented in figure 3. The original span wing weighed nearly 40 lb and with the addition of both nacelles and a wing fin as much as 54.5 lb. The wing was 7.6 ft long with an initial span of approximately 3 ft. The leading-edge sweep was 73° for the inboard 70 percent of the wing and 60° for the remaining 30 percent of the span. The lower swept wingtip region was eliminated by removing sections parallel to the root chord in increments of 10 percent of the original span.

A photograph of the wing alone is presented as figure 4. The wing consisted of a 0.25-in-thick aluminum alloy (7075-T651) plate to which balsa wood was bonded. Cutouts were made to the aluminum plate to obtain a representative stiffness and mass distribution of a typical aircraft wing having a rib and spar construction. The plate thickness and number of cutouts were also chosen to provide the correct stiffness needed for the models to flutter within the TDT operating boundary. A detailed drawing of the cutout patterns with typical dimensions and a photograph of the wing-plate structure are presented as figures 5 and 6, respectively. The balsa wood was contoured to form a 3-percent-thick biconvex airfoil section and was bonded with the grain perpendicular to the plate to minimize its effect on wing stiffness. The two mounting tabs located at the wing root were clamped between a steel block and a steel beam fixture. The wing was constrained at only two points along the root to more closely represent a flexible fuselage, typical of an HSCT design. The steel beam fixture was mounted to the tunnel side-wall turntable and covered with a fiberglass fairing to provide more realistic wing root aerodynamics. An angle-of-attack accelerometer located on the turntable was used to ensure that the model was at an angle of attack of 0°.

The arrow-wing model was tested with and without two flow-through nacelles for each reduction in span. The two nacelles were mounted on the lower surface to simulate wing-mounted engines. Each was constructed of contoured aluminum tubes weighted with lead rings to more realistically represent the inertia of typical engine nacelles. The nacelle geometry, mass, and inertia properties are presented in figure 7.

In addition, both the original and span-reduced wing only and wing with nacelles configurations were tested with a vertical or 45° outboard canted fin mounted on the upper surface of the wing at 68 percent of the span. It was constructed from a solid 0.125-in-thick aluminum plate to which balsa wood was bonded and contoured to form a 3-percent biconvex airfoil shape. The fin geometry, mass, and inertia properties are presented in figure 8. All configurations were tested at an angle of attack of 0° and at Mach numbers ranging from 0.60 to 1.20. A table and graphical representation of the configurations tested are presented in figure 9.

Model Instrumentation

Model instrumentation included six strain-gauge bridges and two wingtip-mounted accelerometers. Their locations are shown in figure 10. The strain-gauge bridges were oriented to measure bending and torsion moments at the two mounting tabs and the tip crank area. The accelerometers were used to measure dynamic response near the wingtip. Instrumentation output was monitored on strip charts and a frequency analyzer to assure safe margins for both static and dynamic loads and to aid in determining the onset of flutter during testing.

Model Vibration Modes

Measured Vibration Modes

The first five natural vibration frequencies were measured for almost all wing configurations while the model was mounted in the TDT. These measured natural frequencies for each configuration are listed in table I. Hand raps at the midwing leading edge and wingtip were used to excite the model and the corresponding time history signals from the two wing-mounted accelerometers were input to a frequency analyzer to obtain model frequency spectrums. For the wing only configuration, each reduction in span raised the frequencies of the first two modes. However, for the wing with nacelles configuration, the frequency of the first mode increased considerably less with each reduction in span, whereas the frequency of the second mode remained nearly constant. Also, the addition of the two nacelles introduced an additional vibration mode which is referred to as the "nacelle pitch mode."

Node line locations corresponding to each measured natural vibration mode were determined for both the wing only (fig. 11) and the wing with nacelles (fig. 12) configurations. An electromagnetic shaker was attached to the wing near the inboard trailing edge to excite each natural vibration mode. A stationary reference accelerometer was attached to

the wing near the tip to obtain the maximum vibration amplitudes. A roving accelerometer was used to survey the vibration amplitudes across the entire upper surface of the model. The outputs of the two accelerometers were sent through phase-matched dual tracking filters and displayed on a two-channel oscilloscope. A Lissajous figure generated by the two signals was monitored to detect phase shifts as the roving accelerometer passed across each node line. It was found that the addition of the fin, vertical or canted, had little effect on node line locations and therefore the node lines for these configurations are not presented in this report.

Analytical Vibration Modes

A finite element model was created of the wing only and the wing with nacelles configurations for each reduction in span and a dynamic structural analysis performed with the MacNeal-Schwendler Corporation (MSC) NASTRAN finite element program (ref. 20). Overall, the calculated results correlated well with the measured results. Analytical models for the wing consisted of 670 (original span) to 580 (30 percent span reduction) quadrilateral (CQUAD4) and triangular (CTRIA3) plate elements. These elements were chosen to model both the aluminum wing-plate and the 3-percent biconvex balsa wood airfoil because they provide both membrane and bending stiffness. A layout of the NASTRAN finite element model is shown in figure 13. Elements representing balsa wood were superimposed on the elements representing the aluminum plate. Due to variations in the material properties of balsa wood, it was necessary to adjust the density and stiffness of these elements to obtain an analytical model more representative of the physical model. The density of the elements representing balsa wood was adjusted so that the mass of the finite element model was the same as that of the experimental model. The stiffness of these elements was then varied until the natural frequency of the second mode (reference mode) was the same as for the experimental model. The analytical total mass and inertial properties of the wing correlated well with the measured values as shown in the following table:

	Measured	Analytical
Wing mass, slugs . . .	1.242	1.246
c.g.,(x, y), in.	(63.1,9.8)	(62.1,9.3)
I_{XX}, slug-ft^2		0.6441
I_{YY}, slug-ft^2	4.914	4.726
I_{ZZ}, slug-ft^2	5.423	5.370

Analytical frequencies and node line locations for the wing only configuration are compared with measured frequencies and node lines for each reduction in span in table I(a) and figure 11.

The nacelles were modeled separately with CQUAD4 elements and attached to the wing finite element model. The layout of finite elements representing the nacelles is also presented in figure 13. Analytical frequencies and node line locations for the wing with nacelles configuration are compared to measured frequencies and node lines in table I(b) and in figure 12.

The wing fin was also modeled separately using both CQUAD4 and CTRIA3 plate elements (fig. 13). Because the mass of the balsa wood was negligible, only elements representing the aluminum plate were used. Analysis including the fin was only performed on the original span configurations. The addition of the fin had little effect on the analytical or measured natural frequencies. Analytical frequencies for original span configurations with a vertical fin are compared with measured frequencies in table I.

The finite element analysis provided mode shapes and generalized masses which were used as inputs to the flutter analysis. The analytical mode shapes for the wing only and wing with nacelles configurations are presented in figure 14.

Flutter Analysis

The Flutter Analysis System (FAST) computer program described in reference 21 was used to solve for flutter solutions. The flutter analysis was performed to provide a better understanding of the model flutter mechanisms and to evaluate the program's use in predicting arrow-wing flutter phenomenon at Mach numbers between 0.60 and 0.95. The program uses a surface spline to interpolate the displacements and slopes at the downwash collocation points from the calculated mode shapes (ref. 22). The number of collocation points was successively increased from 36 to 144 where it was determined that using more than 100 collocation points had little effect on the calculated flutter results. Figure 15 shows the Gaussian distribution of the 100 collocation points used in the flutter analysis. Next, the generalized unsteady aerodynamic forces are computed at each collocation point with subsonic kernel function theory (ref. 23). Flutter speeds are then calculated at various densities for a particular Mach number by an incremental damping approach (V-G method). From these calculations, a matched point solution is found which gives the correct density and flutter frequency for a given flutter velocity. Because this program uses subsonic kernel function theory to calculate the generalized aerodynamic forces, its

use should be limited to cases where only subsonic flow exists. The good correlation obtained above $M = 0.90$ between analytical and experimental data could be attributed to the wing's thin airfoil and high reduced frequencies ($b\omega_2/V_f > 0.4$) encountered for this model.

Flutter analyses were performed for the wing only and the wing with nacelles configurations with FAST for each reduction in span. Because this method considers the wing to be a thin flat plate (no airfoil shape), the aerodynamic effects of the airfoil shape and nacelles were not included in the analysis. Input to the flutter analysis included the wing planform geometry, calculated mode shapes, calculated generalized masses, and the measured natural frequencies. Measured frequencies were used in the flutter analysis because they were considered to be more representative of the experimental model. Both analytical and experimental flutter results indicated that the first two vibration modes (first bending and first torsion) were the primary modes coupling to produce flutter. The first four vibration modes for the wing only configuration and first five vibration modes for the wing with nacelles configuration were used in the flutter analysis. It was determined that the use of additional modes had a negligible effect on the calculated flutter solutions. A typical structural damping value of 0.01 was used in the analyses for each vibration mode. Match-point flutter solutions were calculated for Mach numbers of 0.60, 0.70, 0.80, 0.90, and 0.95. Flutter analyses were not conducted on any configurations which included a wing fin. Results obtained from wind-tunnel tests conducted on a similar model showed that the addition of a wing-mounted vertical fin had little effect on flutter results (ref. 24). The addition of a fin also had little effect on the natural frequencies (experimental or analytical) of the original span wing and the wing with nacelles.

Wind-Tunnel Test Procedure

The flutter boundaries were approached conservatively and "peak hold" subcritical response data (ref. 10) were evaluated at various Mach number increments. The peak hold method involved analyzing frequency response data from the wing-mounted accelerometers and recording peak amplitudes for each dominant vibration frequency. Flutter projections were made based on plotted data of the inverse of the peak amplitudes versus tunnel dynamic pressure. The inverse amplitude should approach zero as the flutter condition is neared. It should be noted, however, that this was used only as a guideline in predicting the onset of flutter during testing. All flutter boundaries presented in this report consist of flutter points defined both visually and by monitoring dynamic response on a strip chart recorder. When flutter occurred, it was usually necessary to activate the tunnel bypass valves which would rapidly reduce the test-section dynamic pressure to a safe level before destructive wing deflections were encountered.

The tunnel operating procedure used to obtain the flutter boundaries presented in this paper is shown in figure 16. Generally, the first tunnel pass for a new configuration was intended to be free of flutter. Starting at a low stagnation pressure (100–200 psf), the tunnel Mach number and dynamic pressure were gradually increased by increasing the tunnel motor speed. The tunnel speed was increased until either a flutter condition was reached or a maximum test-section Mach number of 1.1–1.2 was obtained (see path 1, fig. 16). If no flutter was encountered, the test-section Mach number was reduced to a safe level and then held constant while the tunnel stagnation pressure was increased by 50–100 psf. Stagnation pressure was increased by bleeding additional R-12 into the tunnel circuit. Again, the tunnel speed was gradually increased (see path 2, fig. 16). This procedure was repeated until the minimum flutter dynamic pressure was established. The same procedure was also used to define the remainder of the flutter boundary (see paths 3–5, fig. 16). Occasionally, flutter points were obtained at Mach numbers beyond the minimum flutter dynamic pressure. This was accomplished by first reducing the tunnel stagnation pressure to a value that would allow an increase in Mach number beyond the minimum flutter dynamic pressure. Mach number was then held constant and additional R-12 was bled into the tunnel circuit to gradually increase dynamic pressure until flutter occurred (see path 6, fig. 16).

Results and Discussion

The experimental and analytical flutter data are presented in tables II and III, respectively. These data tables include Mach number M, dynamic pressure q, frequency f_f, velocity V_f, density ρ, reference length b, mass ratio μ, flutter-speed index V_I, Reynolds number Re, model mass m_o, reference frequency f_2, and frequency ratio f_f/f_2 for each flutter point obtained throughout the test. The reference volume of the test medium v_r ranged from 37.01 ft^3 for the original span wing to 36.02 ft^3 for the wing configurations with a 30-percent reduction in span. Flutter-speed index is a nondimensional velocity parameter frequently used to correlate flutter results obtained for different models. Its value, which is proportional to the square root of dynamic pressure,

depends on the flow conditions, structural stiffness, and planform geometry.

Experimental flutter results are presented as flutter dynamic pressure, frequency ratio, mass ratio, and flutter-speed index versus Mach number in figures 17 through 27. Analytical flutter results are compared with experimental results (q vs M) in figures 18 and 20. These flutter boundaries represent neutral flutter stability. All test configurations had a similar flutter behavior and no unusual flutter mechanisms were encountered. However, the dominant vibration mode in the flutter mechanism varied between the low transonic region ($M \approx 0.70$) and the high transonic region ($M \approx 1.00$). Flutter points in the low transonic region were dominated by the wing first-torsion mode and involved considerable midwing leading-edge deflections. The higher transonic flutter points were dominated by the wing first-bending mode and were characterized by large wingtip deflections. This was even more pronounced in the configurations with nacelles.

Wing Only Configuration

Experimental results showing the effects of reducing the span by 10, 20, and 30 percent on the wing only configuration are presented in figure 17. These results are presented for a Mach number range from 0.73 to 1.01. The dynamic pressure flutter boundary was raised with each successive reduction in span. The greatest increases were observed in the high transonic region. Similar increases in the flutter frequency ratio due to span reduction also were observed in the high transonic region. No significant changes were observed in the mass ratio or the flutter-speed index with each reduction in span.

The subsonic kernel function results for the wing only configuration are presented along with experimental results in figure 18. The analytical flutter dynamic pressure boundaries correlated reasonably well with the experimental flutter boundaries, although the analytical boundaries are conservative (10–25 percent) in the low transonic region. However, for the configuration with 30 percent span reduction, the analysis was slightly nonconservative ($\approx$10 percent) in the high transonic region. The calculated values for flutter-speed index, frequency ratio, and mass ratio given in table III correlated well with the experimental flutter results throughout the transonic region.

Wing With Nacelles Configuration

Experimental results showing the effects of reducing the span by 10, 20, and 30 percent on the wing with nacelles configuration are presented in figure 19. These results are presented for a Mach number range of 0.67 to 1.13. Both the flutter dynamic pressure and flutter-speed index boundaries were raised with each reduction in span. Reducing the span by 30 percent raised the flutter dynamic pressure boundary 50 percent in the lower transonic region and 130 percent in the higher transonic region. The flutter frequency ratio remained nearly constant in the low transonic region but increased in the high transonic region as the span was reduced. The mass ratio, unlike the flutter frequency ratio, decreased substantially in the high transonic region for the larger reductions in span. This may indicate that the high transonic portion of the boundary was influenced more by mass ratio than the lower transonic portion of the flutter boundary. The same trends that were observed in the flutter dynamic pressure boundaries were observed in the flutter-speed index boundaries with the largest increases due to span reduction occurring near Mach 1.

The subsonic kernel function results for the wing with nacelles configuration are presented along with experimental flutter results in figure 20. The same trends that were observed in the experimental flutter dynamic pressure boundaries were observed in the analytical flutter boundaries. Namely, the boundary for analytical flutter dynamic pressure was raised with each reduction in span with the largest increases occurring at $M = 0.95$. The calculated values for flutter-speed index, frequency ratio, and mass ratio listed in table III correlated well with the experimental flutter results throughout the transonic region.

Wing Only Versus Wing With Nacelles Configuration

Experimental results showing the effects of reducing the span by 30 percent on the wing only and the wing with nacelles configurations are presented in figure 21. The plot of dynamic pressure versus Mach number clearly shows that reducing the span had a stabilizing effect on both the wing only and the wing with nacelles configurations. The wing with nacelles configuration, however, was far more sensitive to the reductions in span, particularly in the transonic region. Although the addition of engine nacelles was destabilizing for the original span arrow wing, their addition acted to stabilize the wing once the moderately swept portion of the wing was completely eliminated. The flutter frequency ratio increased as expected with a 30-percent reduction in span for the wing only and the wing with nacelles configurations. Also, the flutter frequency ratio for the wing with nacelles configuration was consistently lower than the

corresponding wing only configuration, particularly in the high transonic region. The mass ratio values decreased with a 30-percent reduction in span. This was most obvious in the transonic region for the wing with nacelles configuration. Reducing the span by 30 percent had little effect on the flutter-speed index boundary for the wing only configuration although it was increased significantly for the wing with nacelles configuration.

Wing With Fin Configurations

Experimental results showing the effects of reducing the span on the wing with fin (vertical and 45° canted) configurations are presented in figures 22 and 23, respectively. These results are presented for a Mach number range of 0.70 to 1.14. For all fin configurations the plotted results have been limited to dynamic pressure and flutter-speed index parameters. Reducing the span raised the flutter dynamic pressure boundary for both the vertical and 45° canted fin configurations, particularly in the high transonic region. However, a slightly greater increase was seen with a 20-percent reduction in span than with a 30-percent reduction below $M = 0.98$ for the vertical fin configuration and below $M = 0.93$ for the 45° canted fin configuration. The flutter-speed index values decreased slightly for both fin configurations in the low transonic region with each reduction in span. Little change in flutter-speed index due to span reduction was observed near Mach 1.

Wing Only Versus Wing With Fin Configurations

Experimental results for the wing only and the wing with fin configurations are presented in figure 24 for the original span and 30 percent span reduction. The addition of a vertical or 45° canted fin had little effect on the flutter dynamic pressure boundary for the original span wing. Their addition was only slightly destabilizing for the wing with 30 percent span reduction. Similar effects were observed for the flutter-speed index boundary.

Wing With Nacelles and Fin Configurations

Experimental results showing the effects of reducing the span on the wing with nacelles and fin (vertical and 45° canted) configurations are presented in figures 25 and 26. These results are presented for a Mach number range of 0.67 to 1.13. Reducing the span raised the flutter dynamic pressure boundary significantly for both the vertical and 45° canted fin configurations. The largest increases in the flutter boundary occurred with the 20- and 30-percent reductions in span. The flutter-speed index also increased with the 20- and 30-percent reductions in span for both fin configurations. However, a slightly greater increase was seen with a 20-percent reduction in span than with a 30-percent reduction above $M = 0.95$ for the 45° canted fin configuration.

Wing With Nacelles Versus Wing With Nacelles and Fin Configurations

Experimental results for the wing with nacelles and wing with nacelles and fin configurations are presented in figure 27 for the original span and wing with 30 percent reduced span. The addition of either a vertical or 45° canted fin had no significant effect on the flutter characteristics of the original span wing with nacelles. However, their addition had a significant effect on the flutter characteristics of the wing with 30 percent reduced span and nacelles. The addition of a vertical fin lowered the flutter dynamic pressure boundary in the high transonic region by 10 percent, whereas the 45° canted fin lowered the entire flutter dynamic pressure boundary 20 to 30 percent. Similar trends in flutter-speed index were also observed for the wing with 30 percent reduced span.

Summary of Results

The present study was undertaken to investigate span reduction effects on the flutter characteristics of several arrow-wing configurations. This sensitivity study was developed to better understand the flutter mechanisms of arrow-wing configurations and to increase the available flutter data base for arrow-wing designs. The model was tested with and without two engine nacelles and/or a vertical or 45° outboard canted fin. The experimental flutter results were obtained for Mach numbers ranging from 0.60 to 1.20. In addition to the wind-tunnel test, flutter analyses were performed to evaluate the ability to predict arrow-wing flutter phenomenon and to provide a better understanding of arrow-wing flutter. Both experimental and analytical flutter results are summarized as follows:

1. All test configurations had a similar flutter behavior and no unusual flutter mechanisms were encountered. The vibration mode dominant in the flutter mechanism varied between the lower transonic and the higher transonic regions. Flutter points in the low transonic region were dominated by the wing first-torsion mode and involved considerable midwing, leading-edge deflections. The high transonic flutter points were dominated by the wing

first-bending mode and were characterized by large wingtip deflections. This was even more evident in the configurations with nacelles.

2. The flutter dynamic pressure boundary was raised with each reduction in span for the wing only configuration. The largest increases were observed in the high transonic region for each reduction in span. Flutter-speed index values remained nearly constant with each reduction in span.

3. Both the flutter dynamic pressure and the flutter-speed index boundaries were raised with each reduction in span for the wing with nacelles configuration. The largest increases were observed in the high transonic region for both the 20- and 30-percent reductions in span.

4. The wing with nacelles configuration was far more sensitive to reductions in span than the wing only configuration, particularly in the high transonic region. This indicates that although the addition of engine nacelles was destabilizing for the original span arrow wing, their addition acted to stabilize the wing once the lower swept outboard region of the wing was eliminated.

5. For all fin configurations (vertical or 45° canted), reducing the span raised the flutter dynamic pressure boundaries. The flutter-speed index boundaries for the wing with fin configurations decreased slightly, whereas the wing with nacelles and fin configurations generally increased for each reduction in span.

6. The addition of a vertical or 45° canted fin to the wing only or wing with nacelles configurations had little effect on the flutter dynamic pressure and flutter-speed index boundaries for either of the original span configurations. The addition of a vertical fin to the 30-percent span-reduced wing with nacelles configuration lowered the flutter dynamic pressure boundary in the high transonic region only. However, the addition of the 45° canted fin lowered the entire flutter dynamic pressure boundary.

7. Overall, the analytical flutter boundaries obtained for the wing only and the wing with nacelles configurations showed the same trends as the experimental flutter boundaries. However, the analysis was consistently more conservative relative to the experimental results in the low transonic region than in the high transonic region.

NASA Langley Research Center
Hampton, VA 23665-5225
March 5, 1991

References

1. Douglas Aircraft Company, New Commercial Programs: *Study of High-Speed Civil Transports.* NASA CR-4235, 1989.

2. McLean, F. Edward: *Supersonic Cruise Technology.* NASA SP-472, 1985.

3. Boeing Commercial Airplane Co.: *Advanced Concept Studies for Supersonic Vehicles.* NASA CR-159028, 1979.

4. Sobieszczanski, Jaroslaw; McCullers, L. Arnold ; Ricketts, Rodney H.; Santoro, Nick J.; Beskenis, Sharon D.; and Kurtze, William L.: Structural Design Studies of a Supersonic Cruise Arrow Wing Configuration. *Proceedings of the SCAR Conference—Part 2,* NASA CP-001, [1977], pp. 659–683.

5. Kordes, Eldon E.: Influence of Structural Dynamics on Vehicle Design—Government View. *A Collection of Technical Papers, Volume B—AIAA 18th Structures, Structural Dynamics and Materials Conference and Dynamics Specialist Conference,* Mar. 1977, pp. 174–176. (Available as AIAA Paper 77-438.)

6. LTV Hampton Technical Center: *Computer Aided Structural Methods With Application to a Supersonic Arrow-Wing Configuration.* NASA CR-132551, 1974.

7. Sobieszczanski-Sobieski, J.; Gross, David; Kurtze, William; Newsom, Jerry; Wrenn, Gregory; and Greene, William: Supersonic Cruise Research Aircraft Structural Studies: Methods and Results. *Supersonic Cruise Research '79—Part 2,* NASA CP-2108, 1980, pp. 617–656.

8. Boeing Commercial Airplane Co., Preliminary Design Dep.: *Study of Structural Design Concepts for an Arrow Wing Supersonic Transport Configuration,* Volume 2. NASA CR-132576-2, 1976.

9. Gordon, C. K.; and Visor, O. E.: *SCAR Arrow-Wing Active Flutter Suppression System.* NASA CR-145147, 1977.

10. Sandford, Maynard C.; Abel, Irving; and Gray, David L.: *Development and Demonstration of a Flutter-Suppression System Using Active Controls.* NASA TR R-450, 1975.

11. Wykes, J. H.; Sweet, H. R.; Joseph, J. A.; and Hodson, C. H.: *Commercial Supersonic Transport Flutter Studies.* ASD-TDR-63-818, U.S. Air Force, May 1964.

12. Sakata, I. F.; and Davis, G. W.: *Evaluation of Structural Design Concepts for an Arrow-Wing Supersonic Cruise Aircraft.* NASA CR-2667, 1977.

13. Ruhlin, Charles L.; and Pratt-Barlow, Charles R.: *Transonic Flutter Study of a Wind-Tunnel Model of an Arrow-Wing Supersonic Transport.* NASA TM-81962, 1981.

14. Doggett, Robert V., Jr.; and Ricketts, Rodney H.: *Effects of Angle of Attack and Vertical Fin on Transonic Flutter Characteristics of an Arrow-Wing Configuration.* NASA TM-81914, 1980.

15. Doggett, Robert V., Jr.; and Ricketts, Rodney H.: Some Experimental and Theoretical Flutter Characteristics of an Arrow-Wing Configuration. *Volume B—Dynamics, Structural Dynamics, AIAA/ASME 18th Structures, Structural Dynamics & Materials Conference,* Mar. 1977, pp. 127–132. (Available as AIAA Paper No. 77-422.)

16. Durham, Michael H.; Cole, Stanley R.; Cazier, F. W., Jr.; Keller, Donald F.; Parker, Ellen C.; Wilkie, W. Keats; and Doggett, Robert V., Jr.: *Parametric Flutter Studies of an Arrow-Wing Configuration—Some Early Results.* NASA TM-100608, 1988.

17. Dansberry, Bryan E.; Rivera, Jose A., Jr.; and Farmer, Moses G.: *An Experimental Study of Tip Shape Effects on the Flutter of Aft-Swept, Flat-Plate Wings.* NASA TM-4180, 1990.

18. Walkley, Kenneth B.; and Martin, Glenn L.: *Aerodynamic Design and Analysis of the AST-200 Supersonic Transport Configuration Concept.* NASA CR-159051, 1979.

19. Reed, Wilmer H., III: *Aeroelasticity Matters: Some Reflections on Two Decades of Testing in the NASA Langley Transonic Dynamics Tunnel.* NASA TM-83210, 1981.

20. *MSC/NASTRAN User's Manual—MSC/NASTRAN Version 65.* MSR-39, MacNeal-Schwendler Corp., Nov. 1985.

21. Desmarais, Robert N.; and Bennett, Robert M.: *User's Guide for a Modular Flutter Analysis Software System (FAST Version 1.0).* NASA TM-78720, 1978.

22. Harder, Robert L.; and Desmarais, Robert N.: Interpolation Using Surface Splines. *J. Aircr.,* vol. 9, no. 2, Feb. 1972, pp. 189–191.

23. Watkins, Charles E.; Woolston, Donald S.; and Cunningham, Herbert J.: *A Systematic Kernel Function Procedure for Determining Aerodynamic Forces on Oscillating or Steady Finite Wings at Subsonic Speeds.* NASA TR R-48, 1959.

24. Durham, Michael H.; Cole, Stanley R.; Cazier, F. W., Jr.; Keller, Donald F.; Parker, Ellen C.; and Wilkie, W. Keats: Experimental Transonic Flutter Characteristics of Supersonic Cruise Configurations. *A Collection of Technical Papers, Part 3—31st AIAA/ASME/ASCE/AHS/ASC Structures, Structural Dynamics and Materials Conference,* Apr. 1990, pp. 1432–1441. (Available as AIAA-90-0979-CP.)

Table I. Measured and Analytical Natural Frequencies

(a) Model configurations without nacelles

Span reduction, percent	Mode 1		Mode 2		Mode 3		Mode 4		Mode 5	
	f_m, Hz	f_a, Hz	f_m, Hz	f_a, Hz	f_m, Hz	f_a, Hz	f_m, Hz	f_a, Hz	f_m, Hz	f_a, Hz
Wing only										
0	6.15	6.3	15.2	15.2	23.5	22.4	35.0	34.2	49.0	48.8
10	7.3	7.5	15.6	15.6	26.2	24.8	39.0	38.4	49.8	49.7
20	9.05	9.3	16.1	16.2	28.7	27.6	46.2	46.1	51.4	51.9
30	10.9	11.5	16.5	16.5	30.2	29.4	53.3	52.1	54.5	55.4
Wing with vertical fin										
0	5.8	5.9	15.0	15.1	23.1	22.2	33.6	33.4	47.3	45.7
10										
20	8.1		16.0		27.7		43.9		50.2	
30	9.4		16.2		28.0		46.0		50.7	
Wing with 45° canted fin										
0	5.7		15.0		23.7		34.5		48.1	
10										
20	7.9		15.9		27.3		42.8		50.4	
30	9.2		16.0		27.7		43.0		51.7	

(b) Model configurations with nacelles

Span reduction, percent	Mode 1		Mode 2		Mode 3		Mode 4		Mode 5	
	f_m, Hz	f_a, Hz	f_m, Hz	f_a, Hz	f_m, Hz	f_a, Hz	f_m, Hz	f_a, Hz	f_m, Hz	f_a, Hz
Wing with nacelles										
0	5.0	5.1	14.1	14.2	17.2	16.5	22.0	20.8	35.5	32.3
10	5.2	5.6	14.1	14.2	20.1	19.2	23.2	22.0	39.5	35.6
20	6.1	6.1	14.2	14.3	21.6	20.3	26.1	24.9	42.0	39.2
30	6.6	6.6	14.3	14.4	22.0	20.8	27.9	26.8	42.6	40.0
Wing with nacelles and vertical fin										
0	4.8	4.9	14.0	14.1	17.2	16.5	22.0	20.6	35.4	32.3
10	5.2		14.1		19.5		23.0		38.5	
20	5.7		14.2		21.4		24.8		42.2	
30	6.2		14.2		21.7		25.8		42.0	
Wing with nacelles and 45° canted fin										
0	4.8		13.9		17.1		21.9		35.7	
10	5.2		14.1		19.4		23.0		38.5	
20	5.7		14.1		21.2		24.7		41.8	
30	6.1		14.2		22.1		25.5		42.5	

Table II. Experimental Flutter Results

(a) Wing only configurations

M	q, psf	f_f, Hz	V_f, fps	ρ, slugs/ft^3	b, ft	μ	$\sqrt{\mu}$	V_I	Re	m_o, slugs	f_2, Hz	f_f/f_2
Wing only, original span												
0.75	188.0	11.4	376.0	0.00266	2.352	11.91	3.45	0.485	3.86×10^6	1.173	15.20	0.75
0.867	182.7	10.86	430.7	0.00197	2.352	16.09	4.01	0.478	3.29	1.173	15.20	0.71
0.965	162.0	9.88	477.7	0.00142	2.352	22.32	4.72	0.450	2.64	1.173	15.20	0.65
0.996	155.2	9.75	490.5	0.00129	2.352	24.57	4.96	0.441	2.47	1.173	15.20	0.64
Wing only, 10 percent span reduction												
0.76	192.0	11.3	381.4	0.00264	2.404	11.79	3.43	0.470	3.87×10^6	1.146	15.65	0.72
0.913	183.0	10.9	454.7	0.00177	2.404	17.59	4.19	0.459	3.12	1.146	15.65	0.70
1.01	170.0	10.4	500.0	0.00136	2.404	22.89	4.78	0.442	2.64	1.146	15.65	0.66
Wing only, 20 percent span reduction												
0.73	209.0	12.7	366.0	0.00312	2.470	9.76	3.12	0.469	4.40×10^6	1.111	16.10	0.79
0.84	203.0	12.28	417.4	0.00233	2.470	13.07	3.62	0.462	3.78	1.111	16.10	0.76
0.93	197.0	11.84	461.5	0.00185	2.470	16.46	4.06	0.455	3.33	1.111	16.10	0.74
1.00	197.4	11.64	493.7	0.00162	2.470	18.79	4.33	0.456	3.13	1.111	16.10	0.72
Wing only, 30 percent span reduction												
0.74	224.0	13.0	370.7	0.00326	2.551	9.14	3.02	0.462	4.66×10^6	1.074	16.55	0.79
0.81	222.0	13.0	404.0	0.00272	2.551	10.96	3.31	0.460	4.26	1.074	16.55	0.79
0.93	211.0	12.5	461.7	0.00198	2.551	15.05	3.88	0.449	3.56	1.074	16.55	0.76

Table II. Continued

(b) Wing with nacelles configurations

M	q, psf	f_f, Hz	V_f, fps	ρ, slugs/ft^3	b, ft	μ	$\sqrt{\mu}$	V_I	Re	m_o, slugs	f_2, Hz	f_f/f_2
Wing with nacelles, original span												
0.67	181.3	10.1	336.1	0.00321	2.352	13.99	3.74	0.431	4.16×10^6	1.662	14.1	0.72
0.75	178.0	9.7	375.1	0.00253	2.352	17.75	4.21	0.427	3.66	1.662	14.1	0.69
0.87	166.3	9.0	432.3	0.00178	2.352	25.23	5.02	0.413	2.98	1.662	14.1	0.64
0.94	144.3	8.2	467.6	0.00132	2.352	34.02	5.83	0.385	2.40	1.662	14.1	0.58
0.97	122.7	7.6	481.2	0.00106	2.352	42.36	6.51	0.355	1.99	1.662	14.1	0.54
0.976	115.0	7.3	484.5	0.00098	2.352	45.82	6.77	0.343	1.85	1.662	14.1	0.52
0.98	104.2	7.0	483.9	0.00089	2.352	50.46	7.10	0.327	1.68	1.662	14.1	0.50
1.01	119.1	7.5	498.1	0.00096	2.352	46.78	6.84	0.350	1.86	1.662	14.1	0.53
Wing with nacelles, 10 percent span reduction												
0.74	196	10.0	372.8	0.00282	2.404	15.75	3.97	0.441	4.03×10^6	1.635	14.1	0.71
0.89	181.6	9.1	443.1	0.00185	2.404	24.01	4.90	0.425	3.17	1.635	14.1	0.65
0.96	143	8.0	476.4	0.00126	2.404	35.25	5.94	0.377	2.32	1.635	14.1	0.57
0.98	118	7.3	488.2	0.00099	2.404	44.87	6.70	0.342	1.88	1.635	14.1	0.52
0.98	114	7.3	487.3	0.00096	2.404	46.77	6.84	0.335	1.83	1.635	14.1	0.52
0.99	119	7.4	492.8	0.00098	2.404	45.32	6.73	0.344	1.88	1.635	14.1	0.52
Wing with nacelles, 20 percent span reduction												
0.75	222	10.1	377.2	0.00312	2.470	14.04	3.75	0.457	4.54×10^6	1.599	14.2	0.71
0.884	222	9.5	437.5	0.00232	2.470	18.89	4.35	0.457	3.97	1.599	14.2	0.67
0.97	191.4	8.6	477.3	0.00168	2.470	26.08	5.11	0.424	3.16	1.599	14.2	0.61
0.977	178.5	8.1	478.4	0.00156	2.470	28.09	5.30	0.410	2.96	1.599	14.2	0.57
1.03	167	8.0	510.8	0.00128	2.470	34.23	5.85	0.396	2.53	1.599	14.2	0.56
1.046	160	8.0	512.1	0.00122	2.470	35.92	5.99	0.388	2.48	1.599	14.2	0.56
1.05	164	8.1	520.6	0.00121	2.470	36.22	6.02	0.393	2.59	1.599	14.2	0.57
Wing with nacelles, 30 percent span reduction												
0.86	272.6	9.9	431.4	0.00293	2.551	14.81	3.85	0.489	4.86×10^6	1.563	14.3	0.69
0.92	263.2	9.4	460.7	0.00248	2.551	17.49	4.18	0.481	4.40	1.563	14.3	0.66
1.00	240.4	8.8	497.8	0.00194	2.551	22.36	4.73	0.459	3.73	1.563	14.3	0.62
1.04	240.7	8.7	518.6	0.00179	2.551	24.23	4.92	0.460	3.60	1.563	14.3	0.61
1.116	240.8	8.6	552.1	0.00158	2.551	27.46	5.24	0.460	3.39	1.563	14.3	0.60
1.13	237	8.5	558.4	0.00152	2.551	28.54	5.34	0.456	3.31	1.563	14.3	0.59

Table II. Continued

(c) Wing with fin configurations

M	q, psf	f_f, Hz	V_f, fps	ρ, slugs/ft^3	b, ft	μ	$\sqrt{\mu}$	V_I	Re	m_o, slugs	f_2, Hz	f_f/f_2
Wing with vertical fin, original span												
0.723	190.6	10.88	361.9	0.00291	2.352	11.16	3.34	0.489	4.03×10^6	1.202	15.0	0.73
0.851	182.4	10.27	423.9	0.00203	2.352	16.00	4.00	0.478	3.32	1.202	15.0	0.68
0.849	181.2	10.23	422.5	0.00203	2.352	16.00	4.00	0.477	3.31	1.202	15.0	0.68
0.972	165.8	9.44	479.9	0.00144	2.352	22.55	4.75	0.456	2.69	1.202	15.0	0.63
1.012	154.5	9.11	497.2	0.00125	2.352	25.98	5.10	0.440	2.44	1.202	15.0	0.61
1.020	155.4	9.07	500.6	0.00124	2.352	26.19	5.12	0.441	2.44	1.202	15.0	0.60
Wing with 45° canted fin, original span												
0.714	198.9	11.00	358.8	0.00309	2.352	10.51	3.24	0.499	4.23×10^6	1.202	15.0	0.73
0.808	191.7	10.63	403.9	0.00235	2.352	13.82	3.72	0.490	3.64	1.202	15.0	0.71
0.877	191.1	10.40	436.1	0.00201	2.352	16.16	4.02	0.489	3.38	1.202	15.0	0.69
0.941	172.3	9.44	467.0	0.00158	2.352	20.56	4.53	0.465	7.86	1.202	15.0	0.63
0.983	165.2	9.23	487.5	0.00139	2.352	23.37	4.83	0.455	2.62	1.202	15.0	0.62
1.000	159.3	9.05	493.2	0.00131	2.352	24.79	4.98	0.447	2.51	1.202	15.0	0.60
1.012	158.1	9.02	501.0	0.00126	2.352	25.78	5.08	0.445	2.45	1.202	15.0	0.60
Wing with vertical fin, 20 percent span reduction												
0.815	215.0	11.90	404.3	0.00263	2.470	11.88	3.45	0.472	4.13×10^6	1.140	16.0	0.74
0.917	212.5	11.10	452.0	0.00208	2.470	15.02	3.88	0.470	3.68	1.140	16.0	0.69
0.951	209.0	11.00	467.8	0.00191	2.470	16.36	4.04	0.466	3.51	1.140	16.0	0.69
0.992	194.4	10.54	486.9	0.00164	2.470	19.05	4.36	0.449	3.14	1.140	16.0	0.66
1.007	188.8	10.54	493.6	0.00155	2.470	20.16	4.49	0.443	3.01	1.140	16.0	0.66
Wing with 45° canted fin, 20 percent span reduction												
0.754	219.3	12.30	375.5	0.00311	2.470	10.05	3.17	0.480	4.50×10^6	1.140	15.9	0.77
0.871	206.1	11.50	432.9	0.00220	2.470	14.20	3.77	0.466	3.68	1.140	15.9	0.72
0.954	195.7	11.00	472.9	0.00175	2.470	17.85	4.22	0.454	3.22	1.140	15.9	0.69
1.001	189.2	10.70	494.1	0.00155	2.470	20.16	4.49	0.446	2.99	1.140	15.9	0.67
1.047	189.9	10.60	513.6	0.00144	2.470	21.70	4.66	0.447	2.90	1.140	15.9	0.67
Wing with vertical fin, 30 percent span reduction												
0.704	209.3	12.75	354.6	0.00333	2.551	9.19	3.03	0.450	4.49×10^6	1.103	16.2	0.79
0.765	210.6		383.8	0.00286	2.551	10.70	3.27	0.452	4.19	1.103	16.2	
0.893	199.0	11.75	447.2	0.00199	2.551	15.38	3.92	0.439	3.40	1.103	16.2	0.73
0.929	197.9	11.75	463.8	0.00184	2.551	16.64	4.08	0.438	3.27	1.103	16.2	0.73
0.996	197.0	11.63	494.7	0.00161	2.551	19.01	4.36	0.437	3.07	1.103	16.2	0.72
1.110	214.9	11.63	546.3	0.00144	2.551	21.26	4.61	0.456	3.06	1.103	16.2	0.72
Wing with 45° canted fin, 30 percent span reduction												
0.764	202.9	12.76	379.3	0.00282	2.551	10.86	3.30	0.435	4.14×10^6	1.103	16.5	0.77
0.835	202.9	12.61	412.9	0.00238	2.551	12.86	3.59	0.435	3.82	1.103	16.5	0.76
0.916	194.5	12.14	451.3	0.00191	2.551	16.03	4.00	0.426	3.37	1.103	16.5	0.74
0.945	204.0	12.28	464.6	0.00189	2.551	16.20	4.02	0.436	3.44	1.103	16.5	0.74
0.990	201.7	12.06	487.1	0.00170	2.551	18.01	4.24	0.434	3.24	1.103	16.5	0.73
0.995	201.3	12.08	488.1	0.00169	2.551	18.11	4.26	0.434	3.25	1.103	16.5	0.73
1.053	215.9	12.18	517.9	0.00161	2.551	19.01	4.36	0.449	3.27	1.103	16.5	0.74
1.143	228.1	12.28	557.1	0.00147	2.551	20.83	4.56	0.462	3.25	1.103	16.5	0.74

Table II. Continued

(d) Wing with nacelles and fin configurations

M	q, psf	f_f, Hz	V_f, fps	ρ, slugs/ft^3	b, ft	μ	$\sqrt{\mu}$	V_l	Re	m_o, slugs	f_2, Hz	f_f/f_2
Wing with nacelles and vertical fin, original span												
0.669	190.6	9.93	335.3	0.00339	2.352	13.48	3.67	0.441	4.35×10^6	1.691	14.0	0.71
0.762	185.1	9.39	381.0	0.00255	2.352	17.92	4.23	0.435	3.73	1.691	14.0	0.67
0.886	169.8	8.65	440.5	0.00175	2.352	26.11	5.11	0.417	2.98	1.691	14.0	0.62
0.957	141.3	7.80	473.6	0.00126	2.352	36.26	6.02	0.380	2.32	1.691	14.0	0.56
0.985	114.9	7.00	486.7	0.00097	2.352	47.10	6.86	0.343	1.84	1.691	14.0	0.50
Wing with nacelles and 45° canted fin, original span												
0.760	186.4	9.31	380.1	0.00258	2.352	17.71	4.21	0.440	3.76×10^6	1.691	13.9	0.67
0.909	165.9	8.25	451.2	0.00163	2.352	28.03	5.29	0.415	2.84	1.691	13.9	0.59
0.964	138.1		475.8	0.00122	2.352	37.45	6.12	0.379	2.26	1.691	13.9	
0.975	122.5	7.16	480.8	0.00106	2.352	43.10	6.57	0.356	1.98	1.691	13.9	0.52
1.032	122.5	7.16	507.8	0.00095	2.352	48.10	6.94	0.356	1.89	1.691	13.9	0.52
Wing with nacelles and vertical fin, 10 percent span reduction												
0.748	203.8	9.70	374.9	0.00290	2.404	15.59	3.95	0.446	4.16×10^6	1.664	14.1	0.69
0.893	186.8	8.60	444.6	0.00189	2.404	23.93	4.89	0.427	3.24	1.664	14.1	0.61
0.956	155.1	7.80	474.1	0.00138	2.404	32.76	5.72	0.389	2.54	1.664	14.1	0.55
0.976	125.4	7.10	481.9	0.00108	2.404	41.86	6.47	0.350	2.02	1.664	14.1	0.50
0.989	122.5	7.09	487.7	0.00103	2.404	43.89	6.62	0.346	1.96	1.664	14.1	0.50
1.003	124.3	7.11	493.7	0.00102	2.404	44.32	6.66	0.348	1.96	1.664	14.1	0.50
1.029	133.5	7.21	506.7	0.00104	2.404	43.47	6.59	0.361	2.06	1.664	14.1	0.51
Wing with nacelles and 45° canted fin, 10 percent span reduction												
0.838	194.9	9.00	417.2	0.00224	2.404	20.18	4.49	0.436	3.60×10^6	1.664	14.1	0.64
0.957	152.7	7.80	473.9	0.00136	2.404	33.24	5.77	0.386	2.51	1.664	14.1	0.55
0.984	118.9	7.00	485.2	0.00101	2.404	44.76	6.69	0.341	1.91	1.664	14.1	0.50
0.997	121.1	7.00	492.1	0.00100	2.404	45.21	6.72	0.344	1.92	1.664	14.1	0.50
1.049	128.0	7.10	513.7	0.00097	2.404	46.60	6.83	0.353	1.96	1.664	14.1	0.50
Wing with nacelles and vertical fin, 20 percent span reduction												
0.850	236.1	9.25	424.5	0.00262	2.470	17.03	4.13	0.467	4.26×10^6	1.628	14.2	0.65
0.948	207.5	8.48	471.1	0.00187	2.470	23.86	4.88	0.438	3.40	1.628	14.2	0.60
0.978	181.9	7.93	486.0	0.00154	2.470	28.97	5.38	0.410	2.89	1.628	14.2	0.56
1.027	157.5	7.54	508.1	0.00122	2.470	36.57	6.05	0.381	2.41	1.628	14.2	0.53
1.047	155.2	7.47	517.3	0.00116	2.470	38.46	6.20	0.378	2.34	1.628	14.2	0.53
1.047	155.0	7.48	517.0	0.00116	2.470	38.46	6.20	0.378	2.33	1.628	14.2	0.53
1.052	161.7	7.52	521.3	0.00119	2.470	37.49	6.12	0.386	2.41	1.628	14.2	0.53

Table II. Concluded

(d) Concluded

M	q, psf	f_f, Hz	V_f, fps	ρ, slugs/ft^3	b, ft	μ	$\sqrt{\mu}$	V_I	Re	m_o, slugs	f_2, Hz	f_f/f_2
Wing with nacelles and 45° canted fin, 20 percent span reduction												
0.728	227.7	10.00	364.4	0.00343	2.470	13.01	3.61	0.462	4.80×10^6	1.628	14.1	0.71
0.810	227.8	9.86	402.7	0.00281	2.470	15.88	3.98	0.462	4.37	1.628	14.1	0.70
0.921	209.2	8.86	455.1	0.00202	2.470	22.09	4.70	0.443	3.58	1.628	14.1	0.63
0.978	171.4	8.00	481.3	0.00148	2.470	30.15	5.49	0.401	2.79	1.628	14.1	0.57
0.986	159.6	7.75	484.5	0.00136	2.470	32.81	5.73	0.387	2.59	1.628	14.1	0.55
1.024	153.9	7.62	500.2	0.00123	2.470	36.27	6.02	0.380	2.43	1.628	14.1	0.54
1.025	154.5	7.70	505.3	0.00121	2.470	36.87	6.07	0.380	2.39	1.628	14.1	0.55
1.049	150.3	7.62	511.3	0.00115	2.470	38.80	6.23	0.375	2.33	1.628	14.1	0.54
1.055	159.1	7.70	519.3	0.00118	2.470	37.81	6.15	0.386	2.40	1.628	14.1	0.55
Wing with nacelles and vertical fin, 30 percent span reduction												
0.813	277.5	9.70	408.2	0.00333	2.551	13.27	3.64	0.492	5.18×10^6	1.592	14.2	0.68
0.922	263.0	9.00	460.5	0.00248	2.551	17.82	4.22	0.479	4.38	1.592	14.2	0.63
0.978	228.7	8.40	486.8	0.00193	2.551	22.89	4.78	0.447	3.62	1.592	14.2	0.59
1.024	223.1	8.20	507.9	0.00173	2.551	25.54	5.05	0.442	3.39	1.592	14.2	0.58
1.048	210.5	8.00	519.5	0.00156	2.551	28.32	5.32	0.429	3.14	1.592	14.2	0.56
1.130	212.1	8.00	558.5	0.00136	2.551	32.49	5.70	0.430	2.95	1.592	14.2	0.56
Wing with nacelles and 45° canted fin, 30 percent span reduction												
0.802	232.2	10.26	403.7	0.00285	2.551	15.50	3.94	0.450	4.37×10^6	1.592	14.2	0.72
0.914	221.2	9.27	456.8	0.00212	2.551	20.84	4.57	0.440	3.70	1.592	14.2	0.65
1.024	188.5	8.41	509.9	0.00145	2.551	30.47	5.52	0.406	2.85	1.592	14.2	0.59
1.049	177.7	8.22	520.9	0.00131	2.551	33.73	5.81	0.394	2.64	1.592	14.2	0.58
1.097	173.8	8.10	538.2	0.00120	2.551	36.82	6.07	0.390	2.54	1.592	14.2	0.57

Table III. Analytical Flutter Results

(a) Wing only configurations

M	q, psf	f_f, Hz	V_f, fps	ρ, slugs/ft^3	b, ft	μ	$\sqrt{\mu}$	V_I	Re	m_o, slugs	f_2, Hz	f_f/f_2
Wing only, original span												
0.6	164	12.5	303.0	0.00357	2.352	8.88	2.98	0.453	4.06×10^6	1.173	15.2	0.82
0.7	170	12.1	353.5	0.00272	2.352	11.65	3.41	0.461	3.61	1.173	15.2	0.80
0.8	173	11.6	404.0	0.00212	2.352	14.95	3.87	0.465	3.22	1.173	15.2	0.76
0.9	167	10.9	454.5	0.00161	2.352	19.69	4.44	0.456	2.75	1.173	15.2	0.72
0.95	159	10.4	479.8	0.00139	2.352	22.8	4.77	0.447	2.51	1.173	15.2	0.68
Wing only, 10 percent span reduction												
0.6	162	13.1	303.0	0.00352	2.404	8.84	2.97	0.431	4.01×10^6	1.146	15.65	0.84
0.7	170	12.7	353.5	0.00272	2.404	11.45	3.38	0.442	3.61	1.146	15.65	0.81
0.8	175	12.2	404.0	0.00215	2.404	14.48	3.81	0.449	3.26	1.146	15.65	0.78
0.9	172	11.4	454.5	0.00166	2.404	18.75	4.33	0.444	2.83	1.146	15.65	0.73
0.95	161	10.9	479.8	0.00140	2.404	22.24	4.72	0.430	2.52	1.146	15.65	0.70
Wing only, 20 percent span reduction												
0.6	169	13.7	303.0	0.00368	2.470	8.27	2.88	0.422	4.20×10^6	1.111	16.1	0.85
0.7	177	13.4	353.5	0.00283	2.470	10.76	3.28	0.431	3.76	1.111	16.1	0.83
0.8	187	12.9	404.0	0.00230	2.470	13.24	3.64	0.444	3.49	1.111	16.1	0.80
0.9	191	12.3	454.5	0.00185	2.470	16.46	4.06	0.448	3.16	1.111	16.1	0.76
0.95	193	12.0	479.8	0.00168	2.470	18.12	4.26	0.451	3.03	1.111	16.1	0.75
Wing only, 30 percent span reduction												
0.6	204	14.0	303.0	0.00444	2.551	6.71	2.59	0.441	5.05×10^6	1.074	16.55	0.85
0.7	204	13.8	353.5	0.00325	2.551	9.17	3.03	0.440	4.32	1.074	16.55	0.83
0.8	215	13.4	404.0	0.00264	2.551	11.29	3.36	0.453	4.01	1.074	16.55	0.81
0.9	227	12.9	454.5	0.00220	2.551	13.55	3.68	0.465	3.76	1.074	16.55	0.78
0.95	237	12.6	479.8	0.00206	2.551	14.47	3.80	0.475	3.71	1.074	16.55	0.76

Table III. Concluded

(b) Wing with nacelles configurations

M	q, psf	f_f, Hz	V_f, fps	ρ, slugs/ft^3	b, ft	μ	$\sqrt{\mu}$	V_I	Re	m_o, slugs	f_2, Hz	f_f/f_2
Wing with nacelles, original span												
0.6	157	10.8	303.0	0.00343	2.352	13.09	3.62	0.402	3.90×10^6	1.662	14.1	0.77
0.7	161	10.3	353.5	0.00257	2.352	17.47	4.18	0.406	3.41	1.662	14.1	0.73
0.8	157	9.6	404.0	0.00193	2.352	23.27	4.82	0.402	2.93	1.662	14.1	0.68
0.9	140	8.7	454.5	0.00135	2.352	33.26	5.77	0.378	2.30	1.662	14.1	0.62
0.95	120	7.9	479.8	0.00104	2.352	43.18	6.57	0.350	1.87	1.662	14.1	0.56
Wing with nacelles, 10 percent span reduction												
0.6	167	10.9	303.0	0.00364	2.404	12.20	3.49	0.407	4.14×10^6	1.635	14.1	0.77
0.7	174	10.4	353.5	0.00279	2.404	15.92	3.99	0.416	3.70	1.635	14.1	0.74
0.8	173	9.7	404.0	0.00212	2.404	20.95	4.58	0.414	2.93	1.635	14.1	0.69
0.9	159	8.8	454.5	0.00154	2.404	28.84	5.37	0.397	2.63	1.635	14.1	0.62
0.95	139	8.2	479.8	0.00120	2.404	37.01	6.08	0.370	2.16	1.635	14.1	0.58
Wing with nacelles, 20 percent span reduction												
0.6	187	11.3	303.0	0.00408	2.470	10.74	3.28	0.420	4.64×10^6	1.599	14.2	0.80
0.7	199	10.9	353.5	0.00319	2.470	13.74	3.71	0.433	4.24	1.599	14.2	0.77
0.8	204	10.3	404.0	0.00250	2.470	17.56	4.19	0.437	3.79	1.599	14.2	0.73
0.9	198	9.6	454.5	0.00191	2.470	22.94	4.79	0.431	3.26	1.599	14.2	0.68
0.95	183	9.1	479.8	0.00159	2.470	27.56	5.25	0.415	2.87	1.599	14.2	0.64
Wing with nacelles, 30 percent span reduction												
0.6	209	11.7	303.0	0.00455	2.551	9.53	3.09	0.428	5.18×10^6	1.563	14.3	0.82
0.7	232	11.3	353.5	0.00371	2.551	11.69	3.42	0.451	4.93	1.563	14.3	0.79
0.8	247	10.9	404.0	0.00303	2.551	14.32	3.78	0.466	4.60	1.563	14.3	0.76
0.9	257	10.2	454.5	0.00249	2.551	17.42	4.17	0.475	4.25	1.563	14.3	0.71
0.95	257	9.8	479.8	0.00224	2.551	19.37	4.40	0.476	4.04	1.563	14.3	0.69

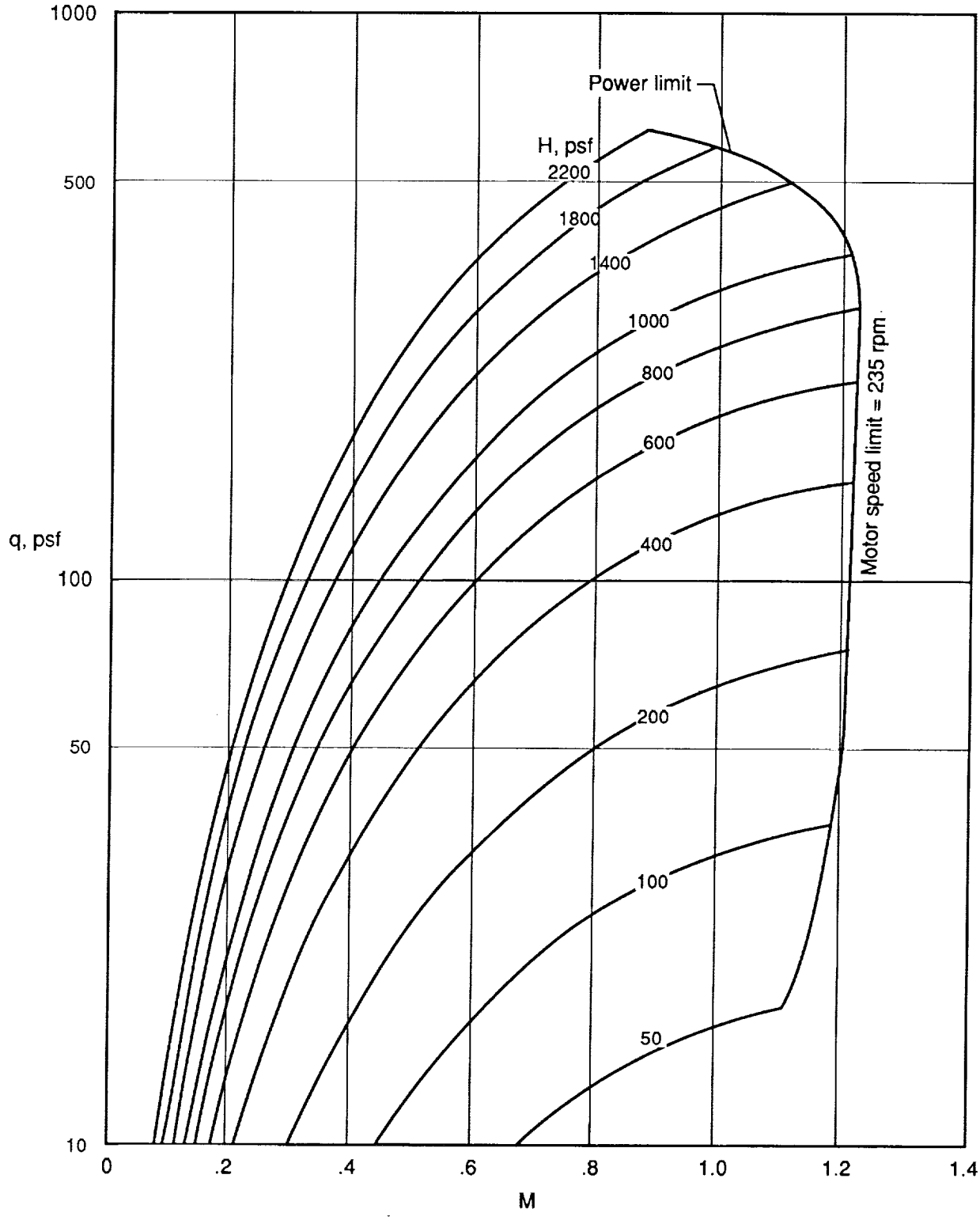

Figure 1. Langley Transonic Dynamics Tunnel operating envelope for R-12.

Figure 2. Original span model with nacelles and vertical fin mounted in Langley Transonic Dynamics Tunnel.

Point	x	y
(1)	0.00	0.00
(2)	91.32	0.00
(3)	91.06	9.71
(4)	93.29	17.89
(5)	108.46	35.06
(6)	98.71	35.06
(7)	80.64	24.62

$S = 1443\ in^2$
$AR = 0.85$

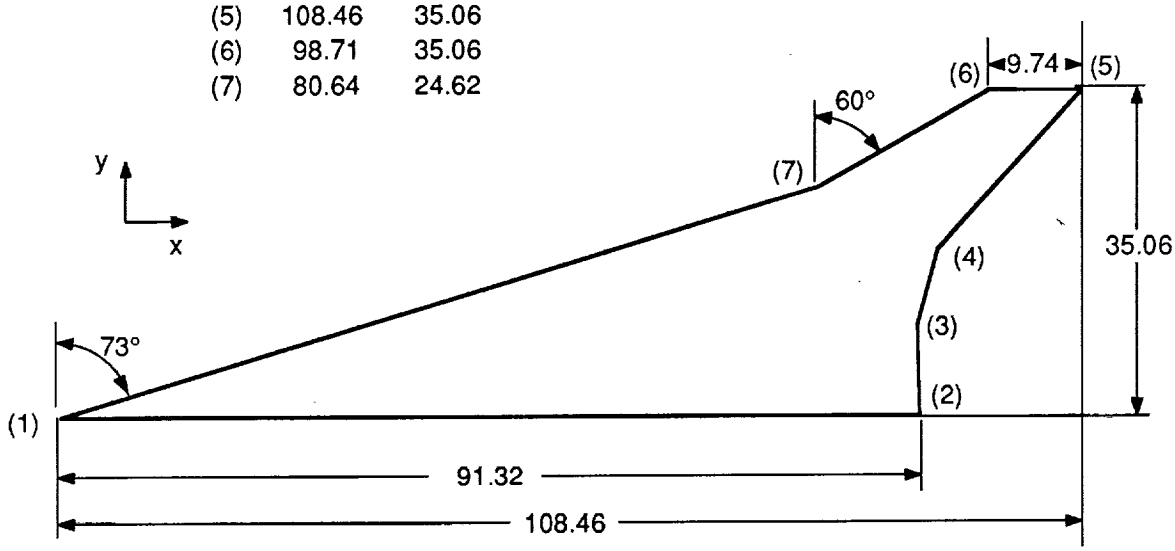

Figure 3. Arrow-wing planform geometry. Linear dimensions are in inches.

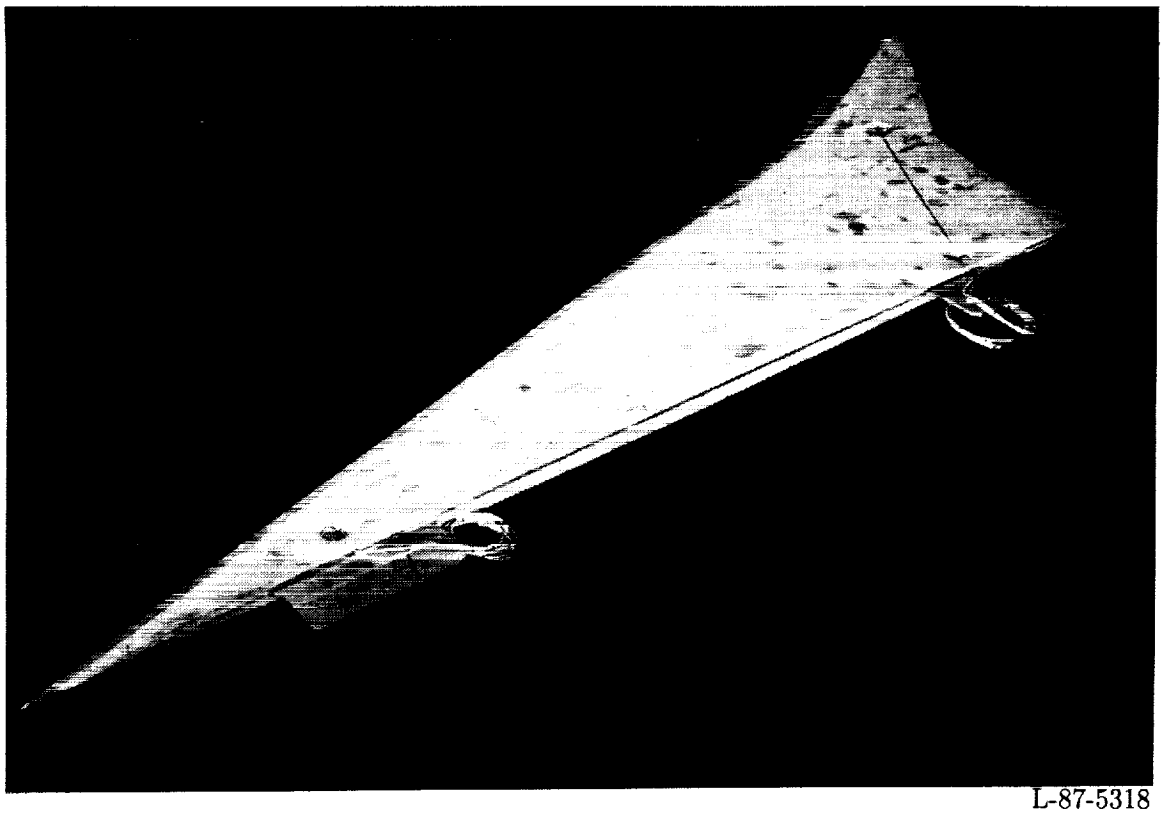

L-87-5318

Figure 4. Arrow wing (without nacelles or fin).

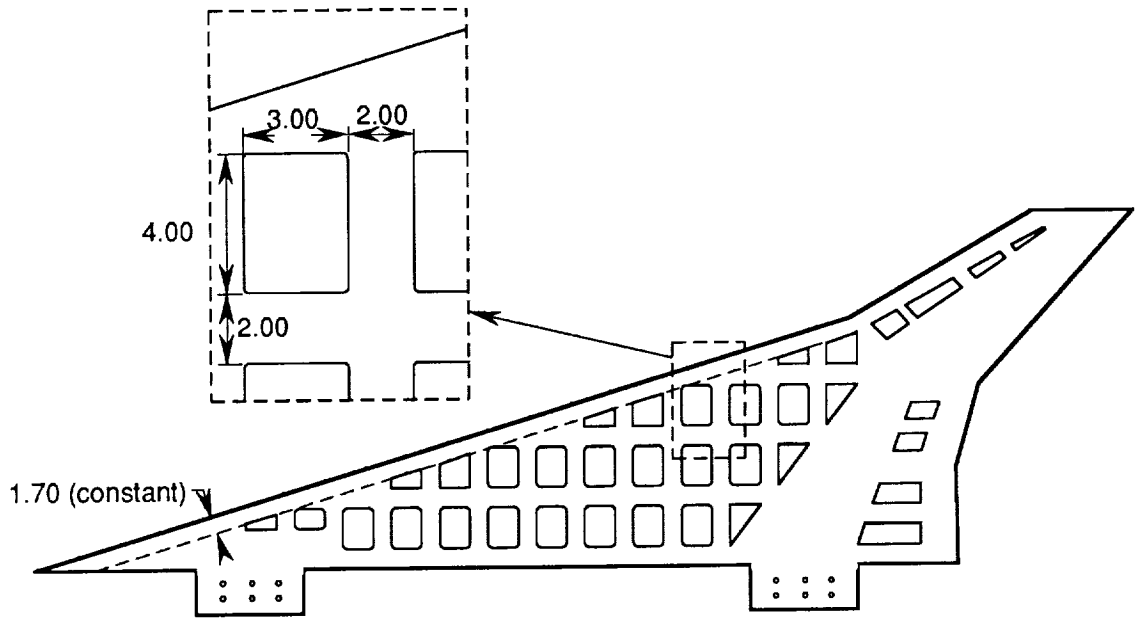

Figure 5. Wing-plate cutout pattern. Dimensions (typical) are in inches.

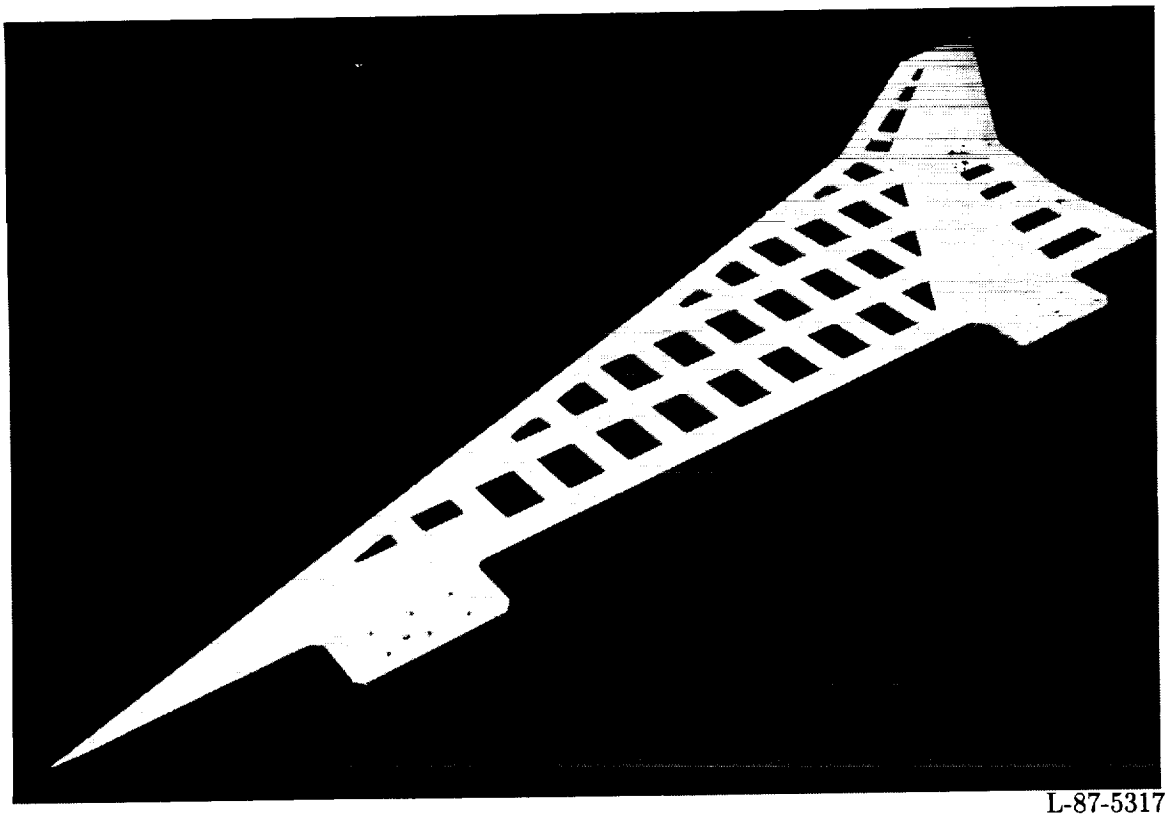

Figure 6. Aluminum wing-plate structure.

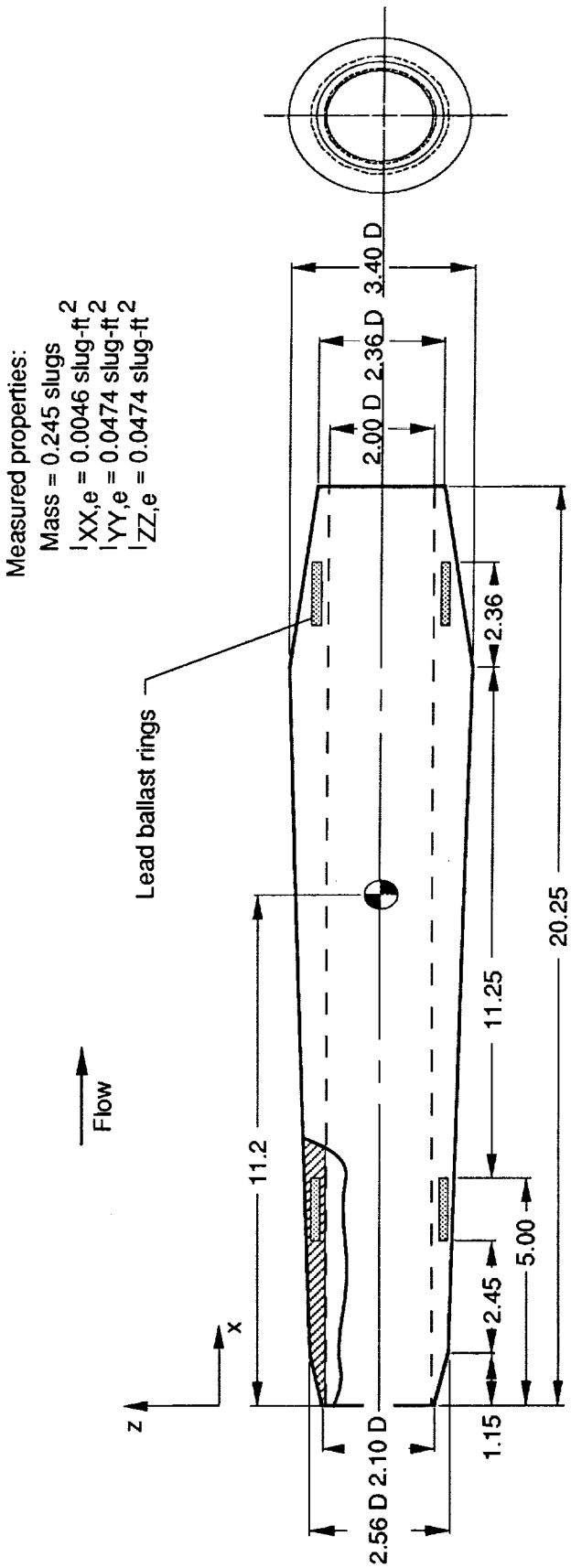

Figure 7. Nacelle geometry. Linear dimensions are in inches.

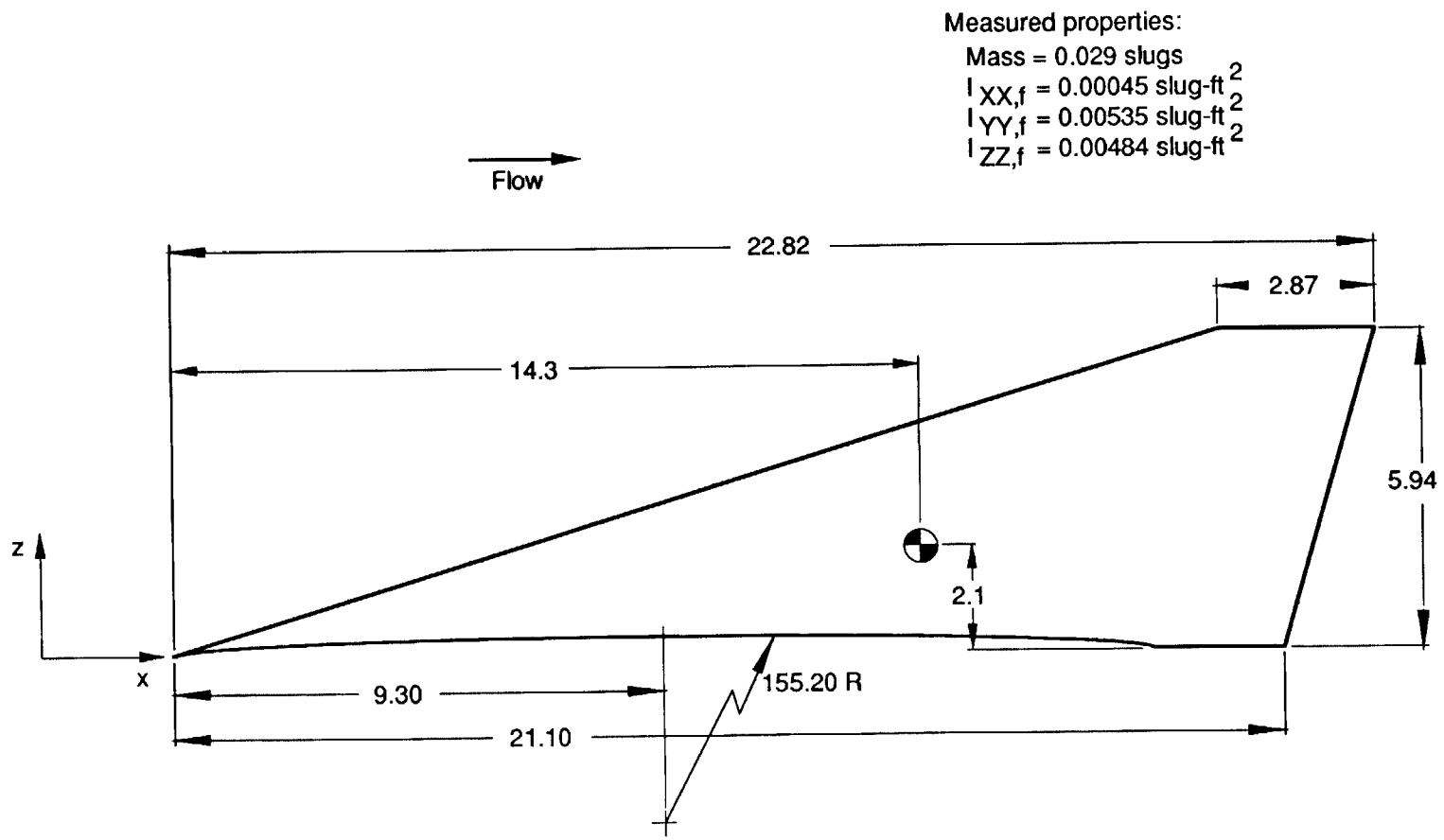

Figure 8. Fin planform geometry. Linear dimensions are in inches.

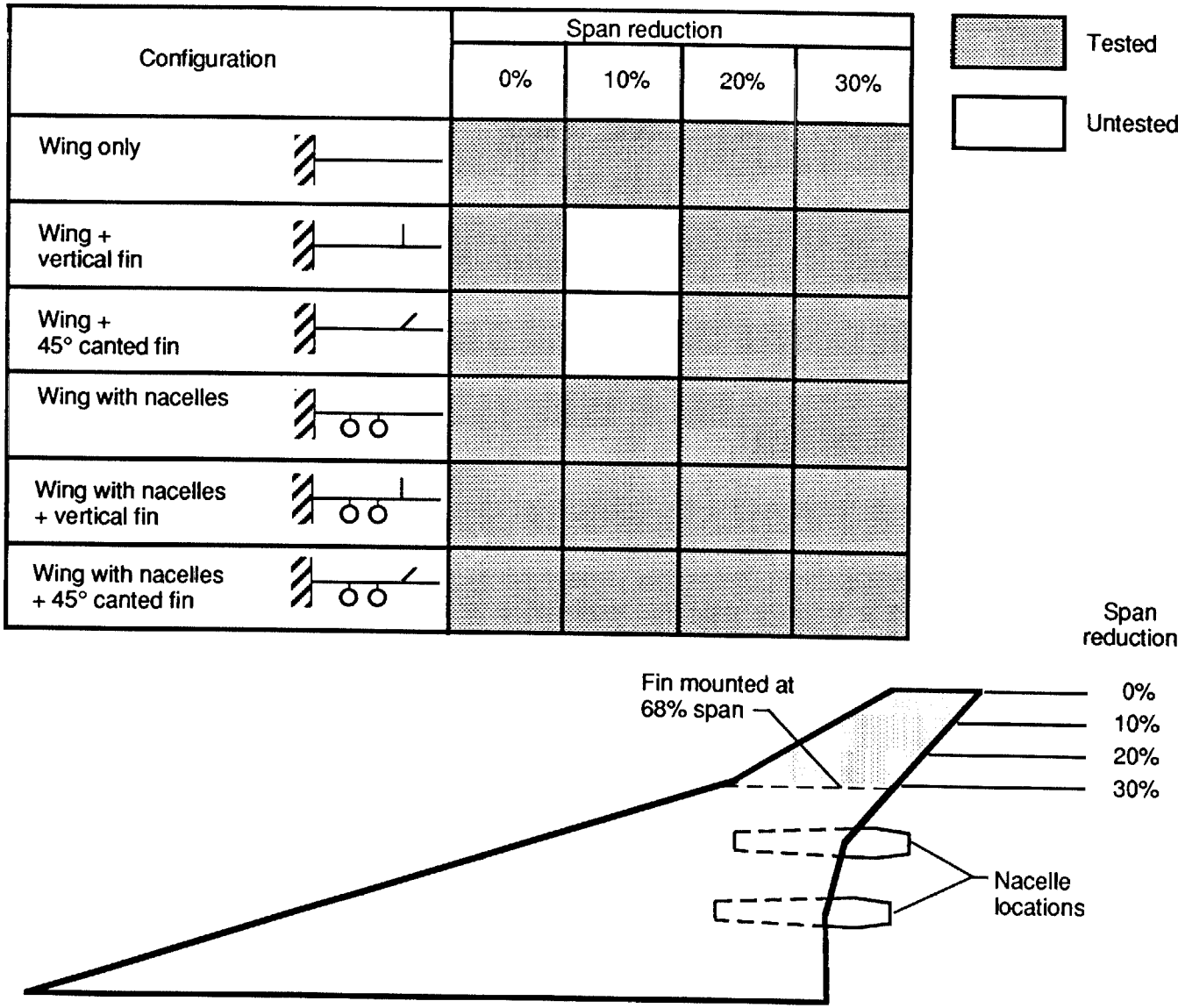

Figure 9. Wind-tunnel test configurations.

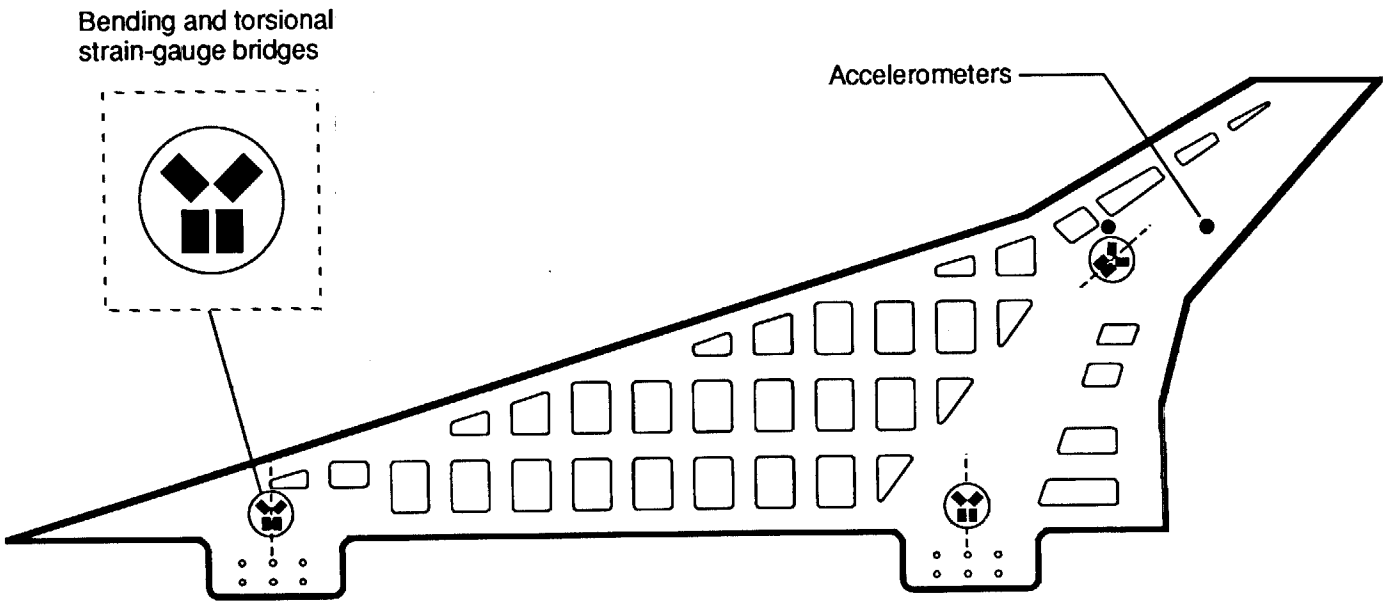

Figure 10. Arrow-wing instrumentation.

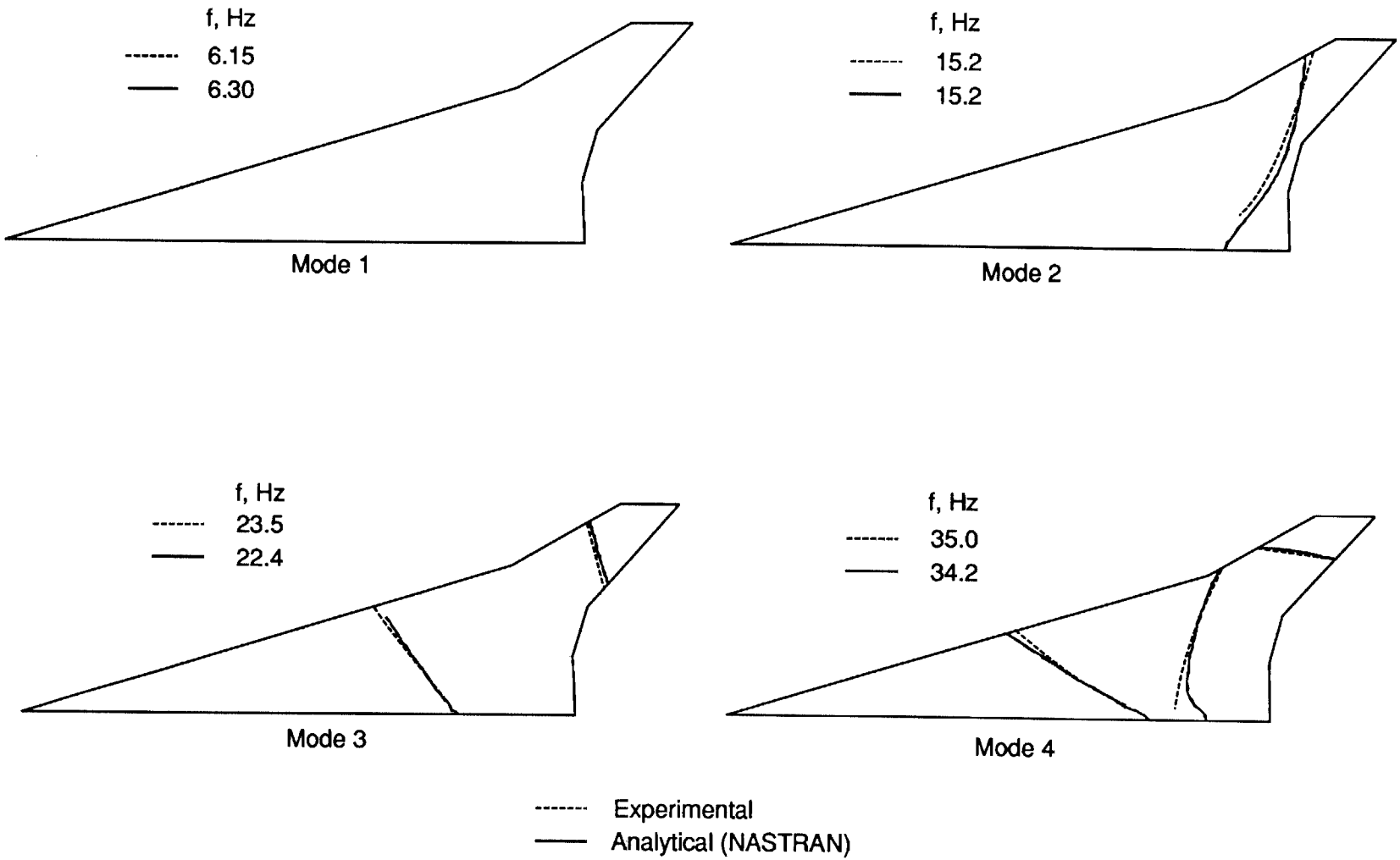

(a) Original span.

Figure 11. Experimental and analytical natural frequencies and node lines for wing only configuration.

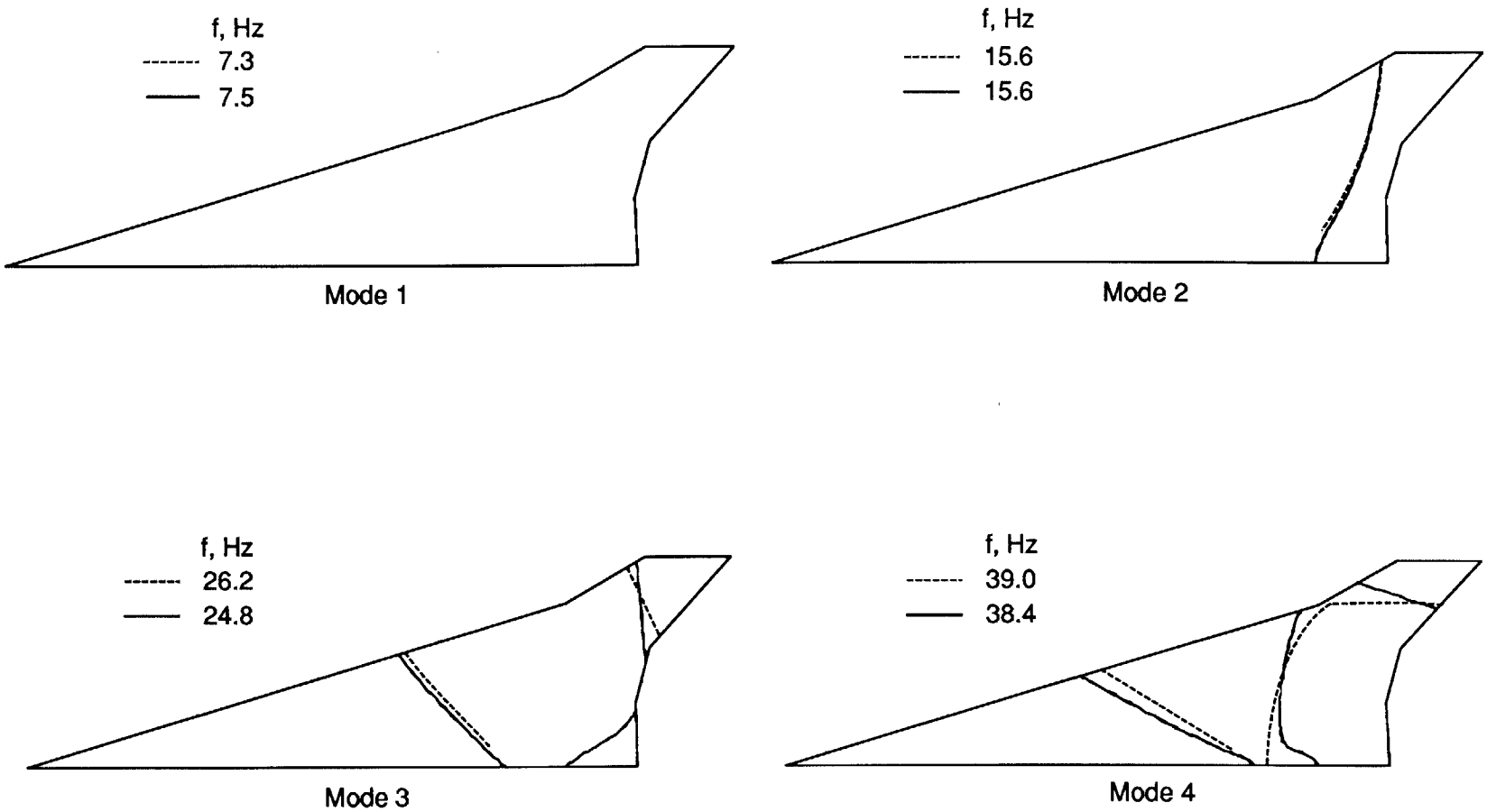

(b) 10 percent span reduction.

Figure 11. Continued.

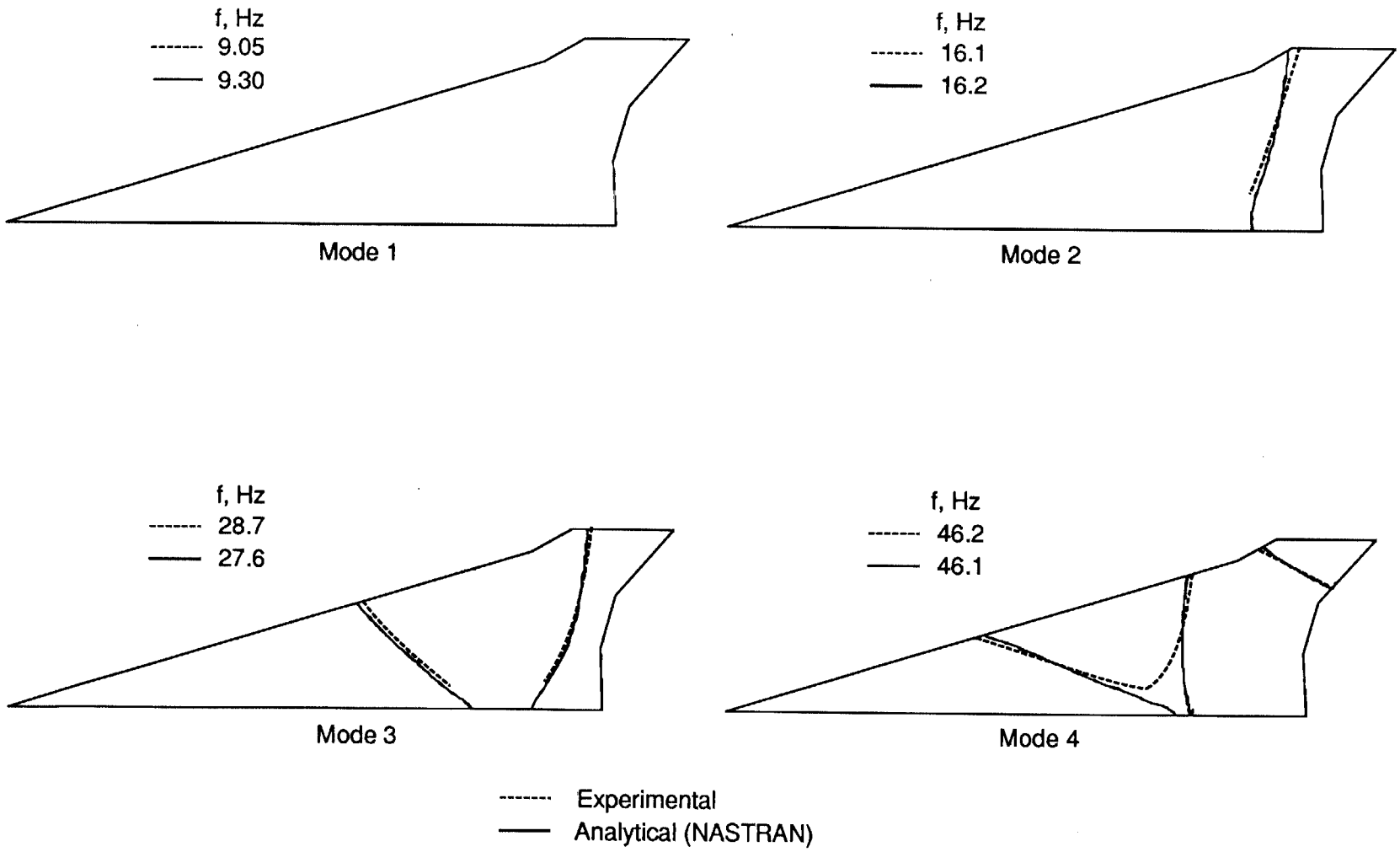

(c) 20 percent span reduction.

Figure 11. Continued.

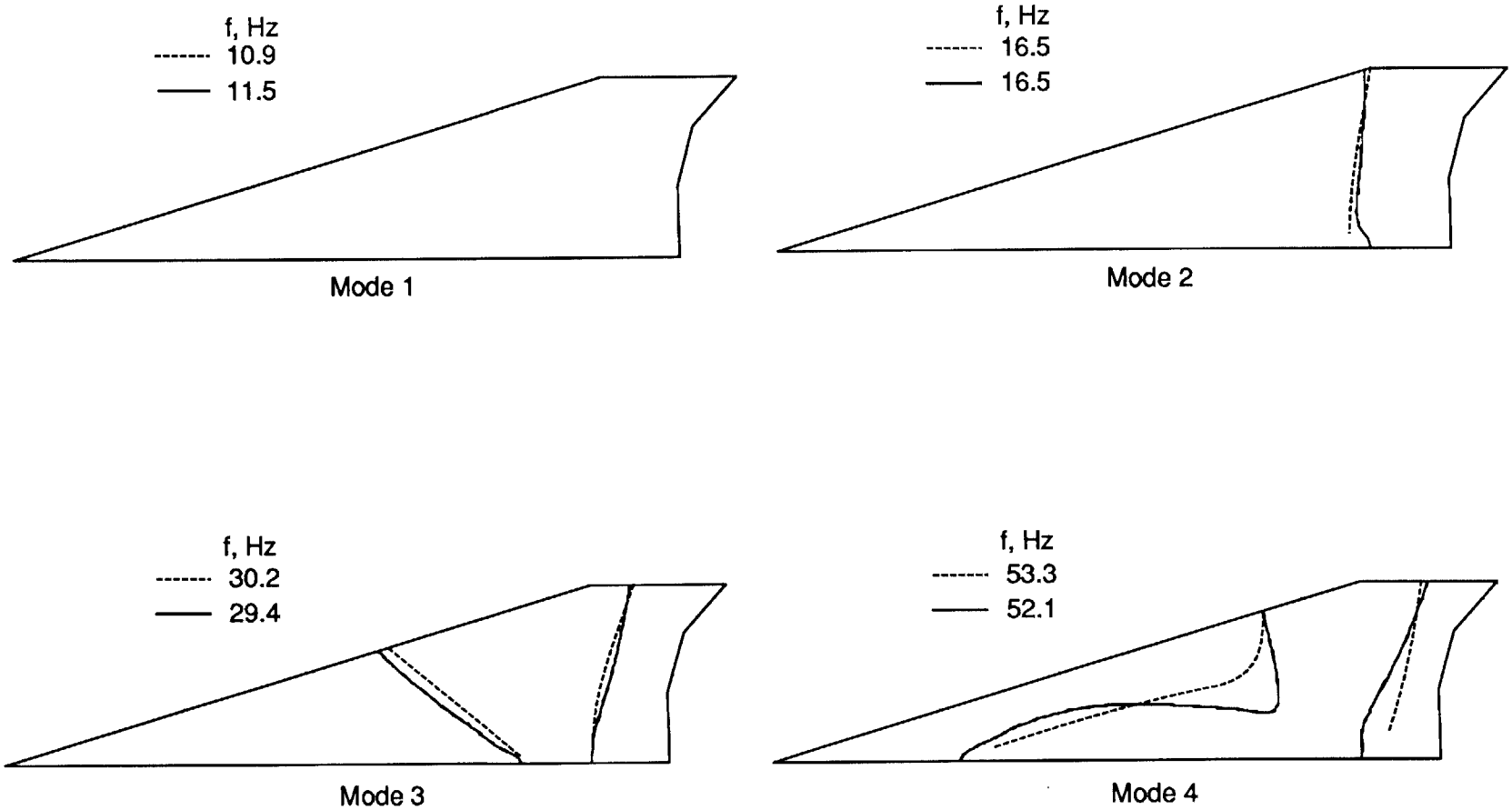

(d) 30 percent span reduction.

Figure 11. Concluded.

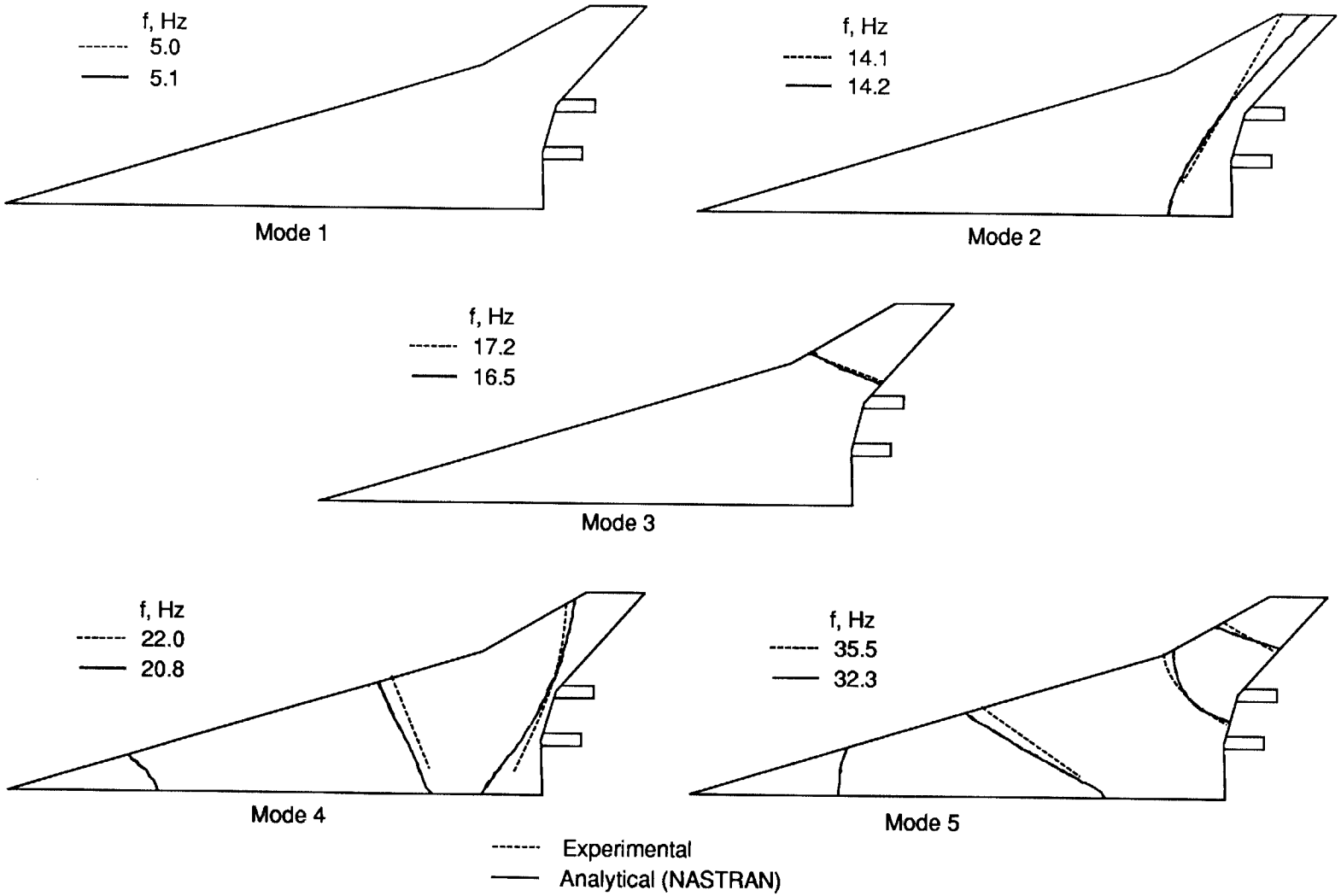

(a) Original span.

Figure 12. Experimental and analytical natural frequencies and node lines for wing with nacelles configuration.

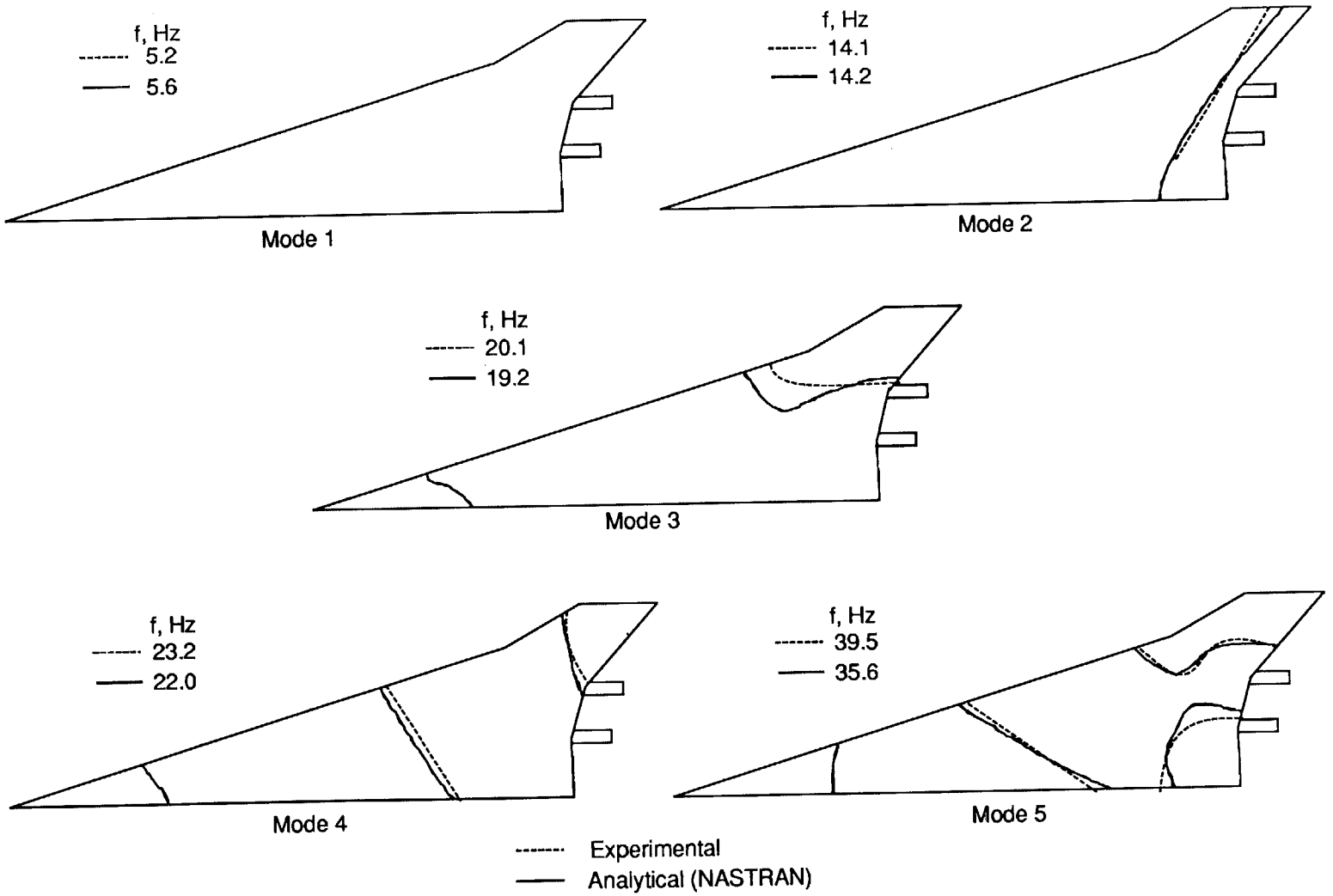

(b) 10 percent span reduction.

Figure 12. Continued.

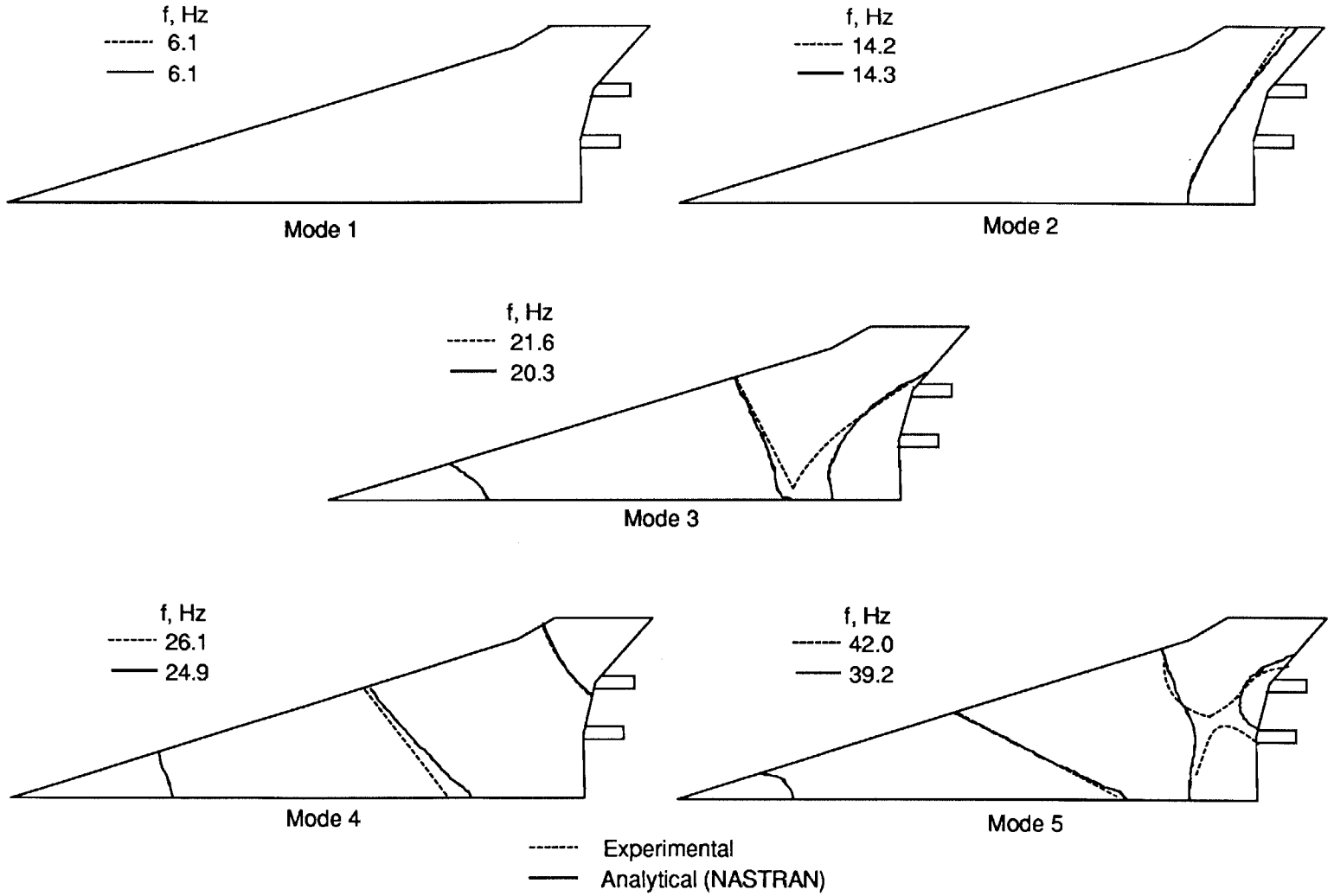

(c) 20 percent span reduction.

Figure 12. Continued.

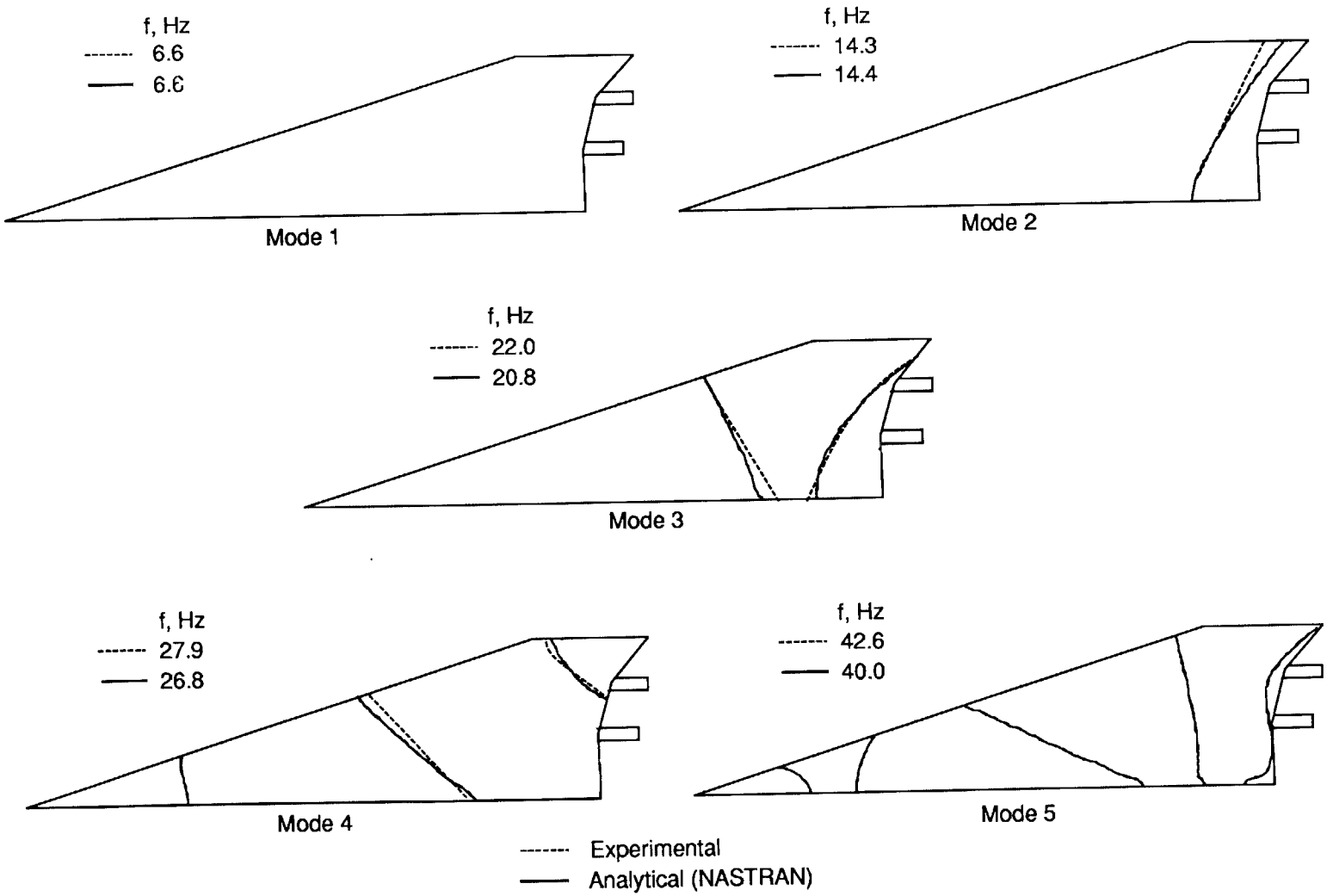

(d) 30 percent span reduction.

Figure 12. Concluded.

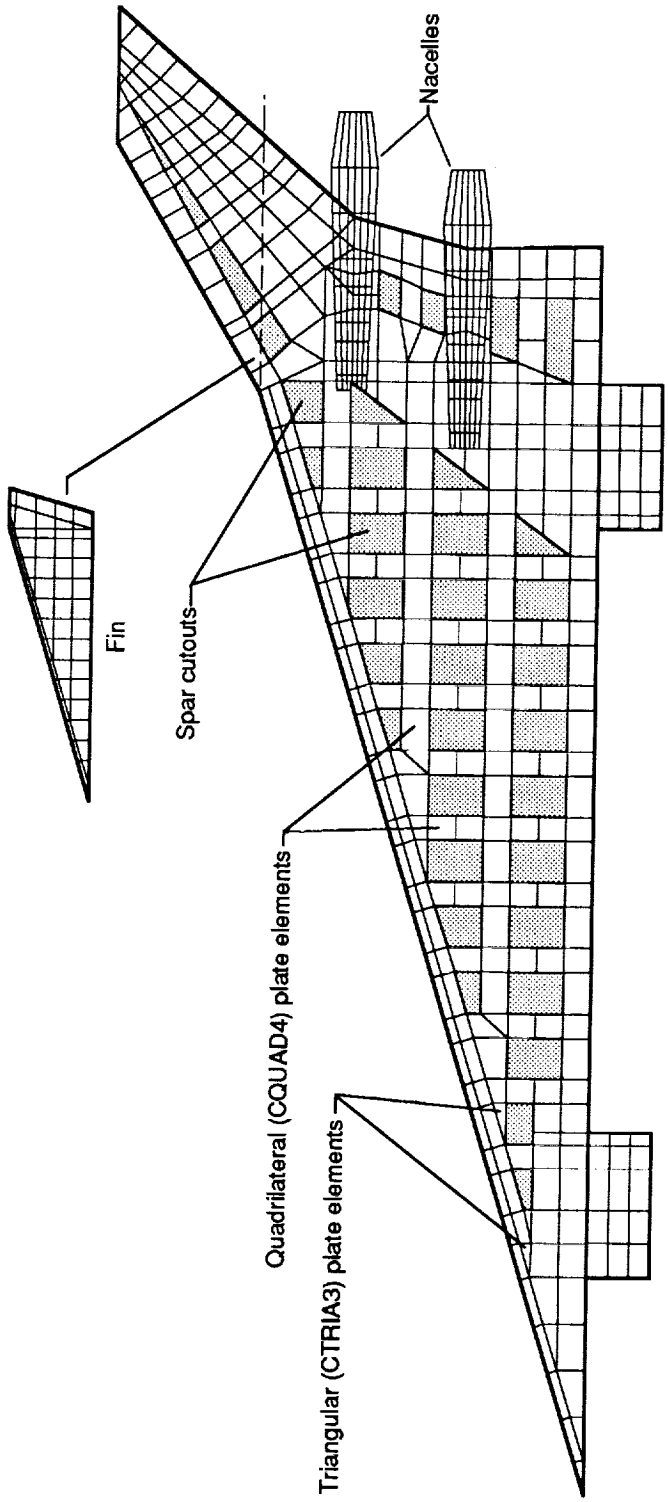

Figure 13. Layout of NASTRAN finite element model.

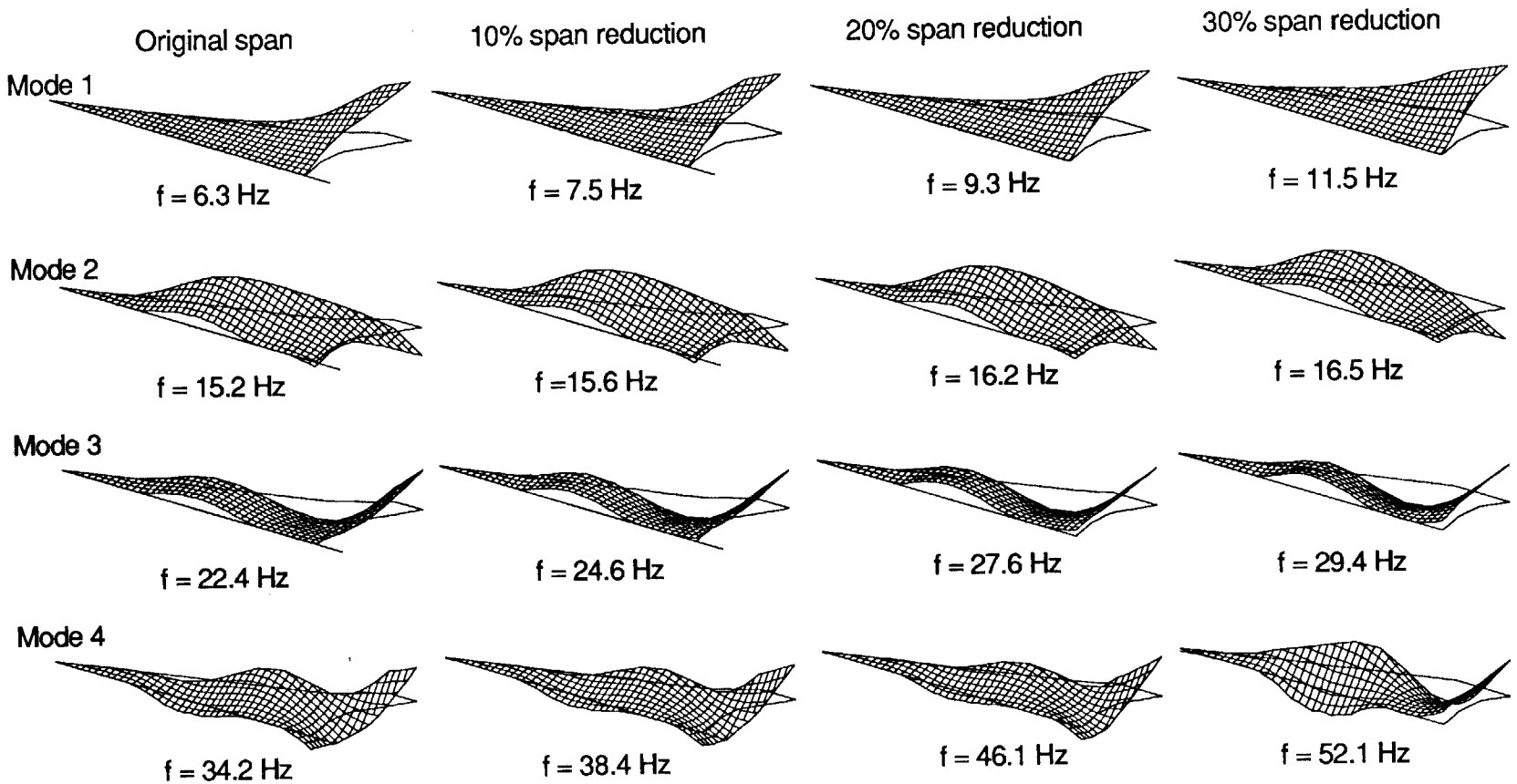

(a) Wing only configuration.

Figure 14. Analytical mode shapes and natural frequencies.

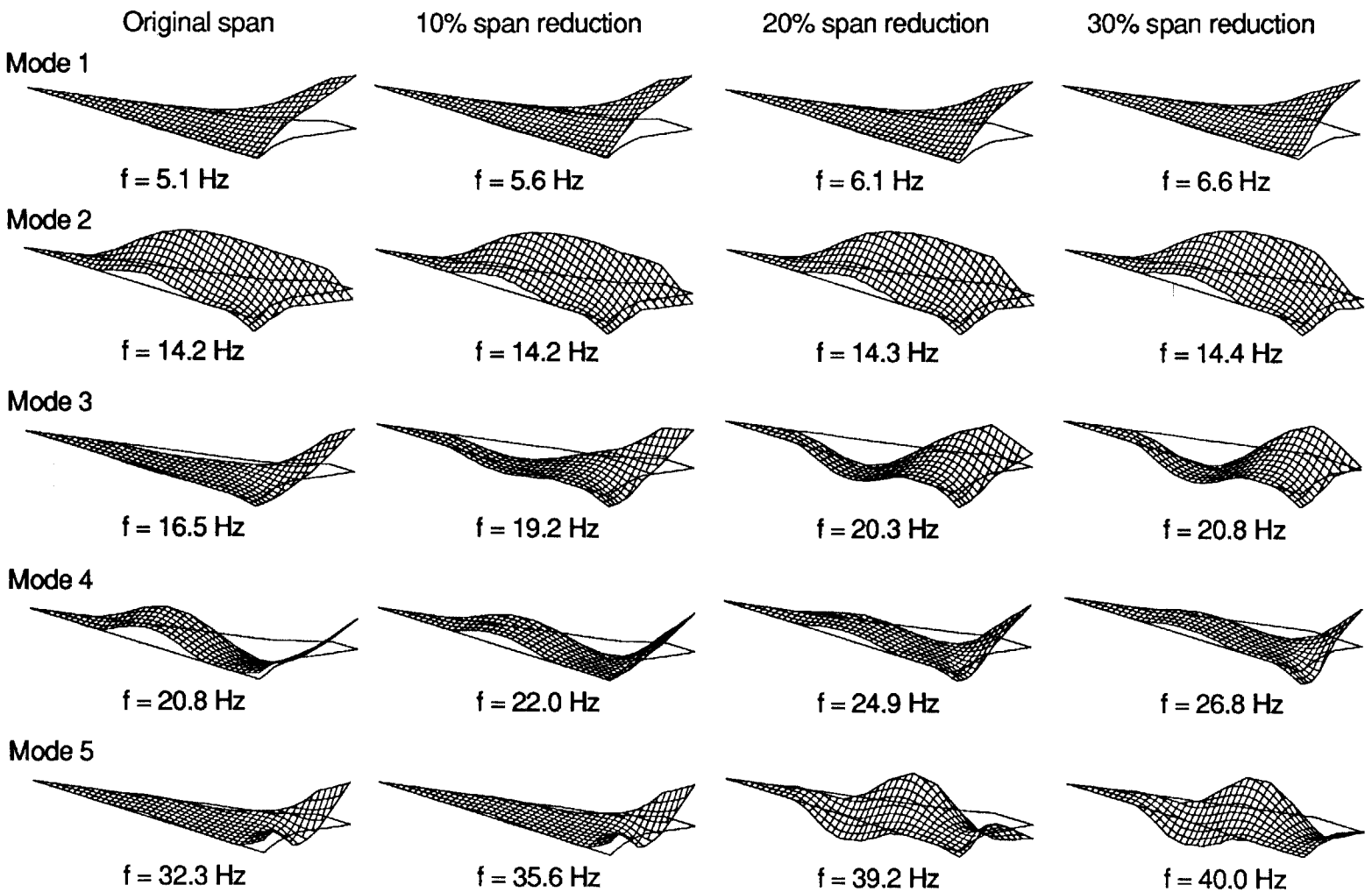

(b) Wing with nacelles configuration.

Figure 14. Concluded.

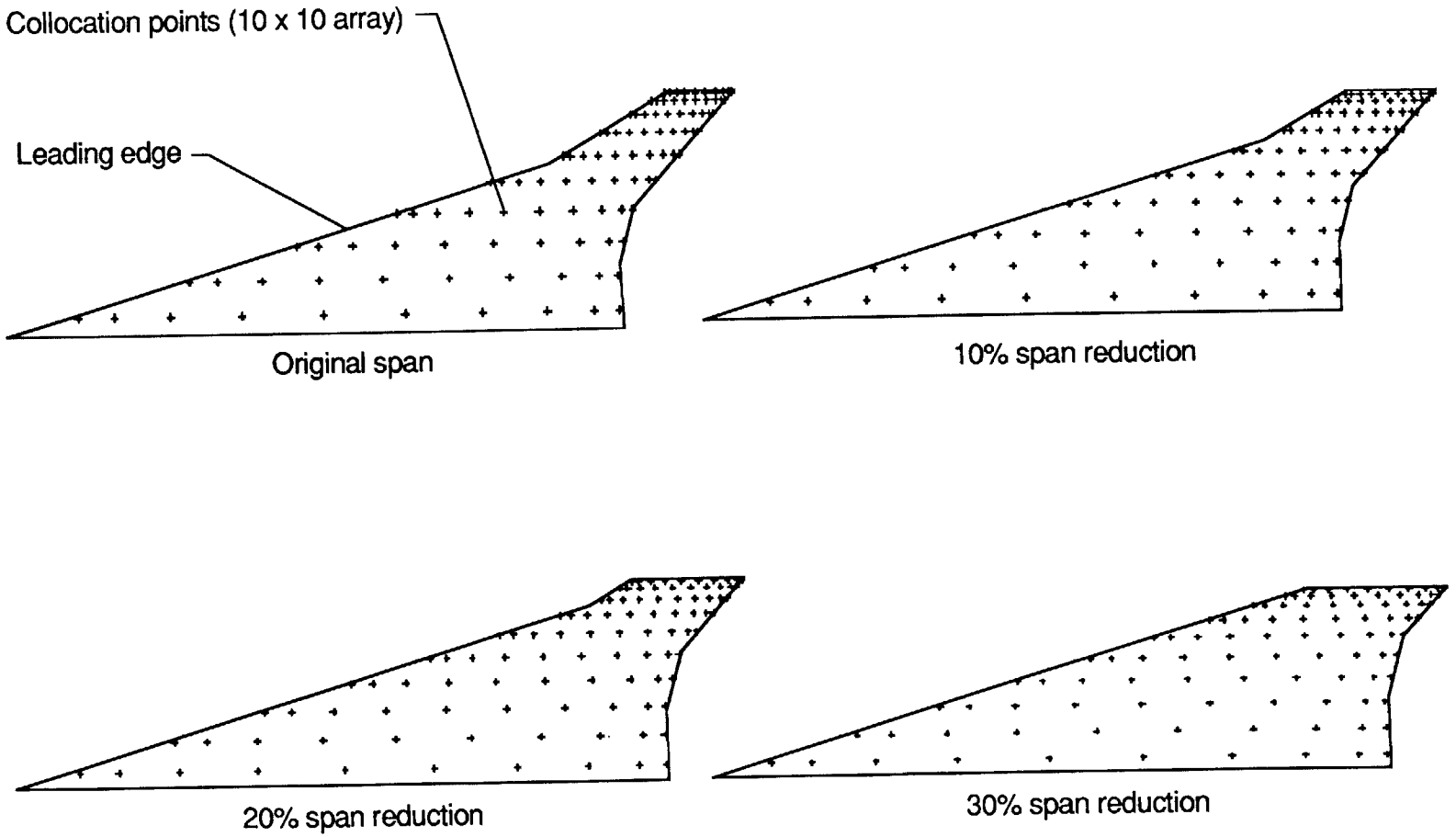

Figure 15. Locations of collocation points for flutter analysis.

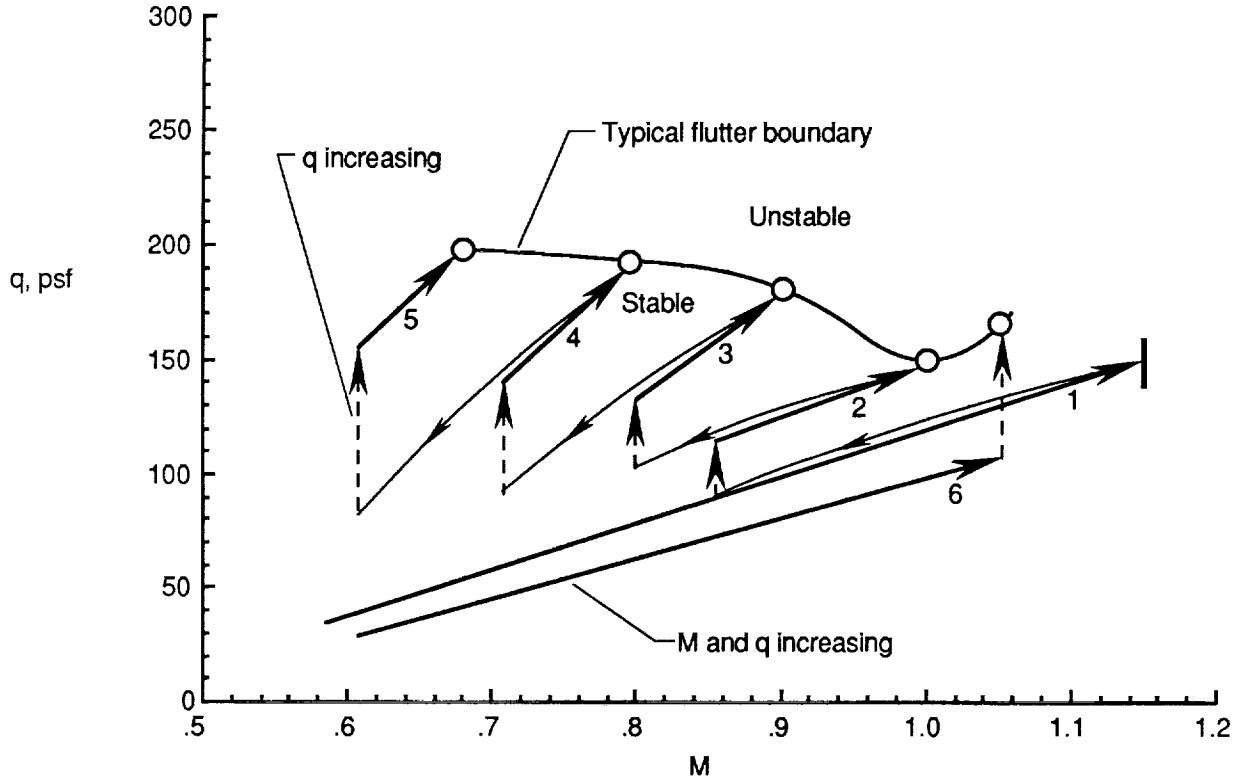

Figure 16. Wind-tunnel operating procedure.

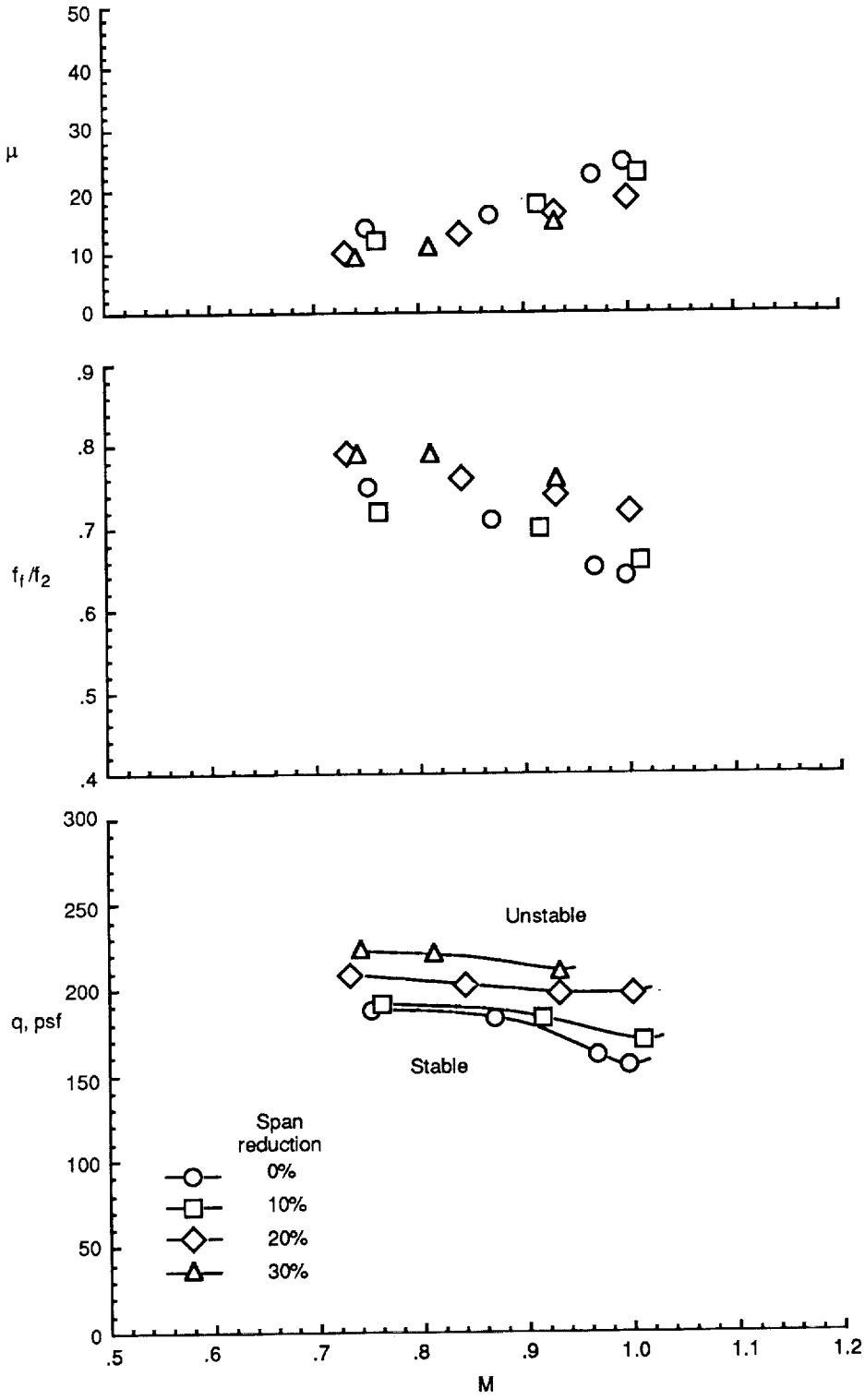

Figure 17. Experimental flutter results for wing only configuration.

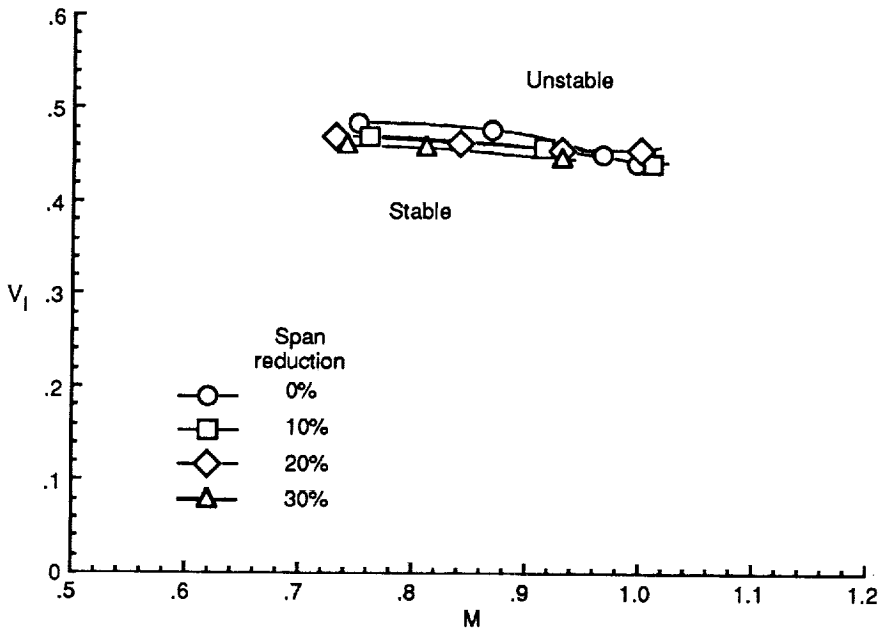

Figure 17. Concluded.

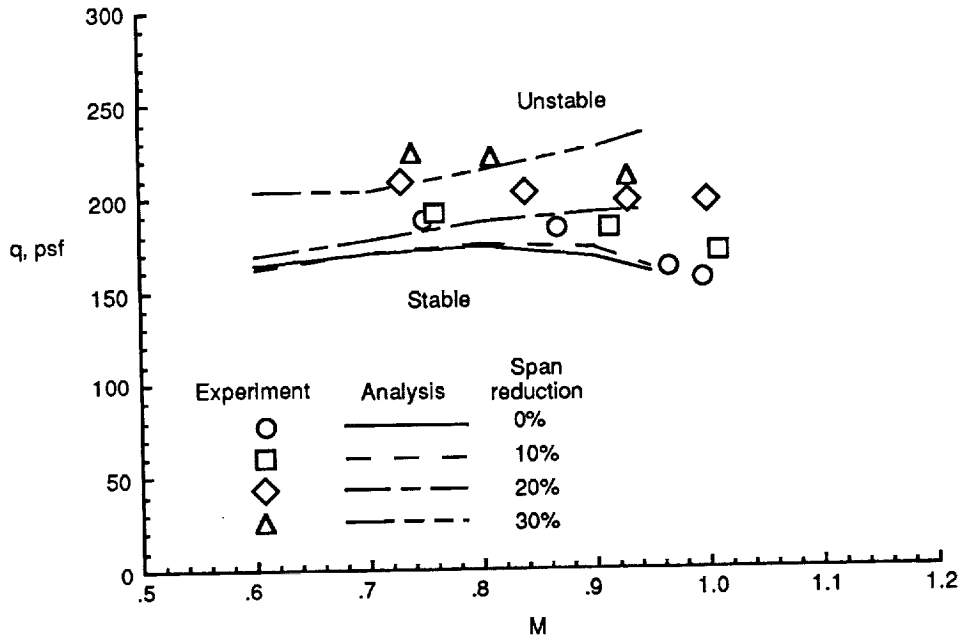

Figure 18. Experimental and analytical flutter dynamic pressure results for wing only configuration.

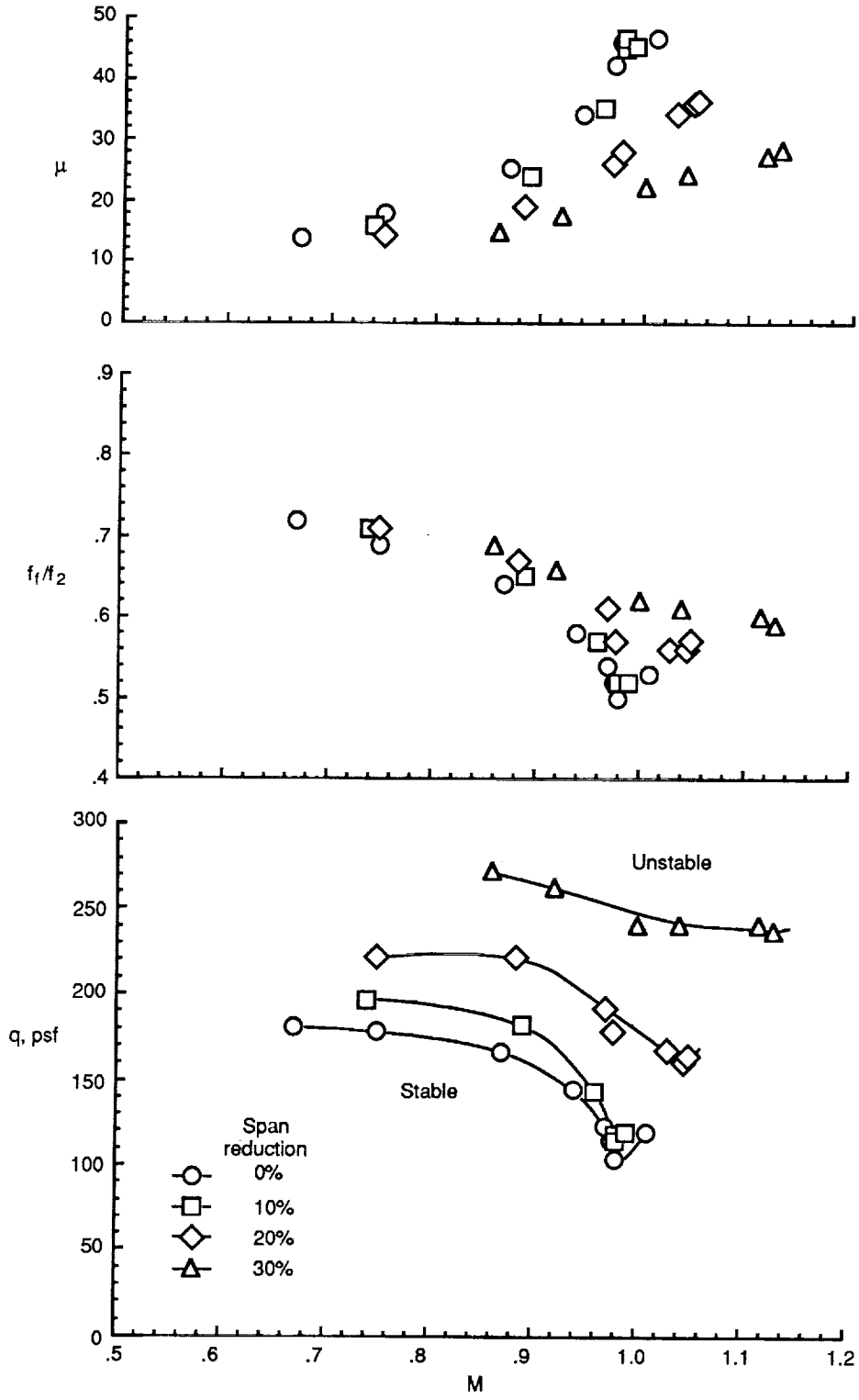

Figure 19. Experimental flutter results for wing with nacelles configuration.

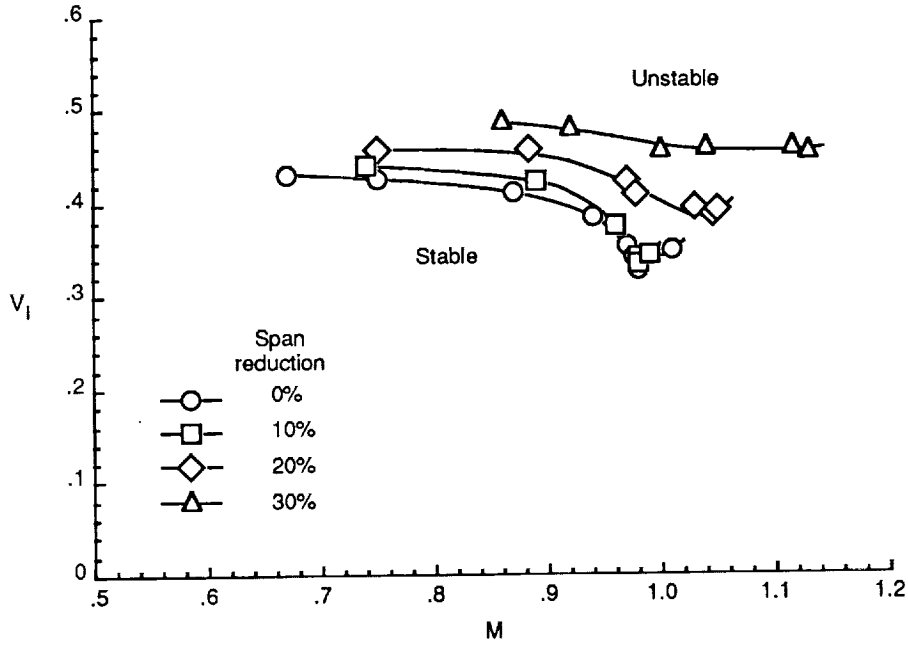

Figure 19. Concluded.

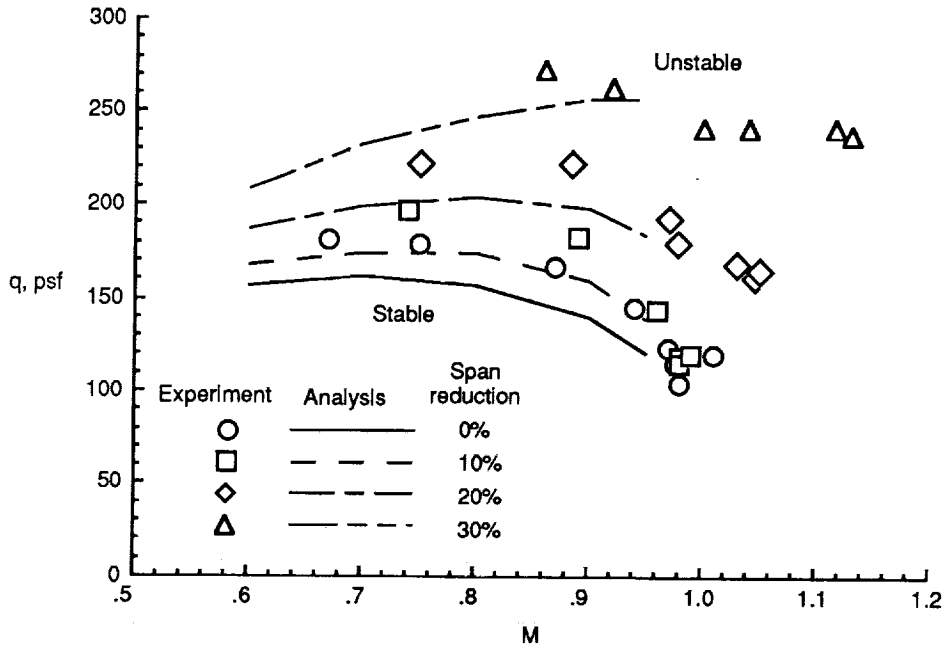

Figure 20. Experimental and analytical flutter dynamic pressure results for wing with nacelles configuration.

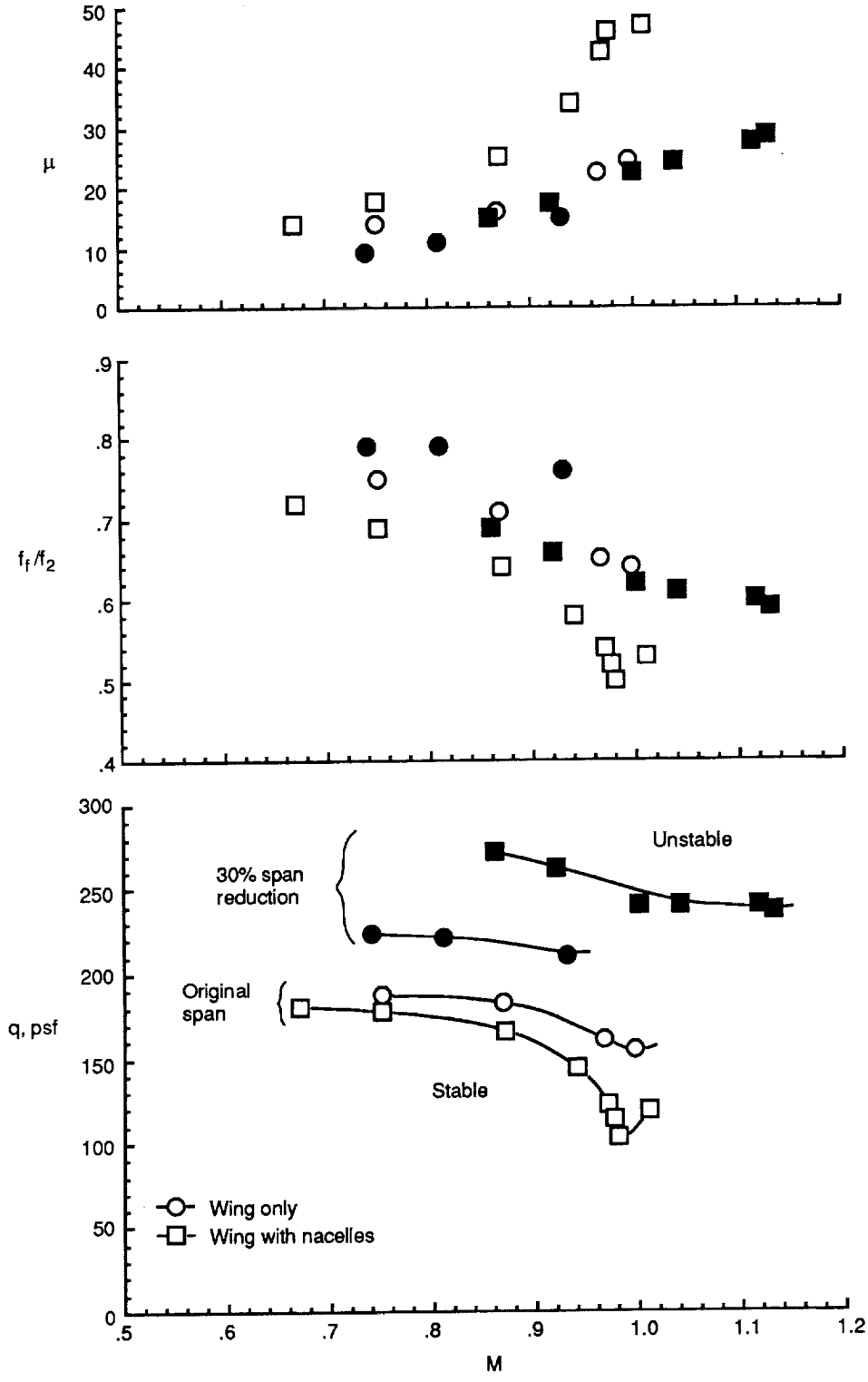

Figure 21. Experimental flutter results for wing only and wing with nacelles configurations (original span and 30 percent span reduction).

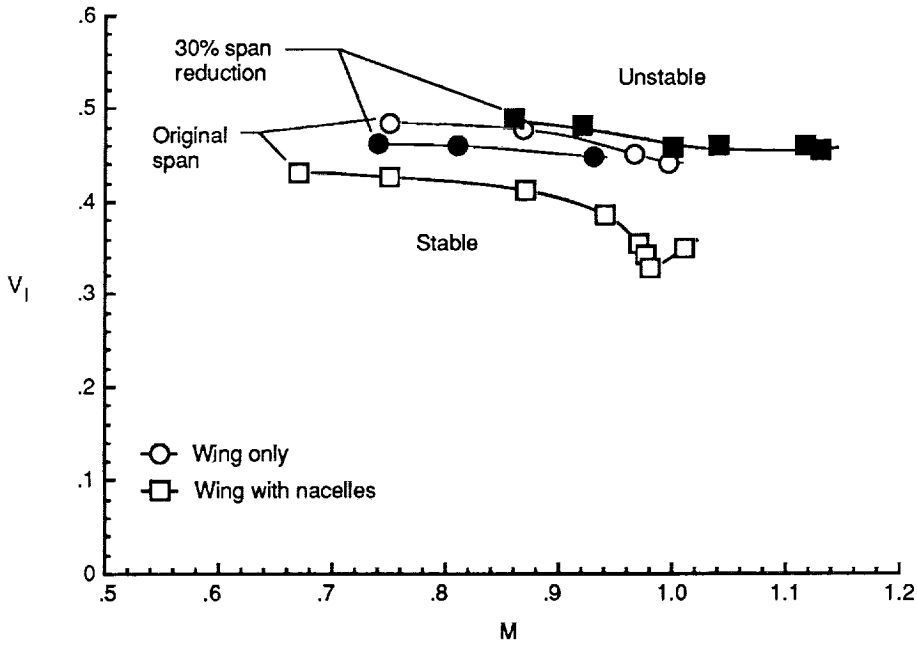

Figure 21. Concluded.

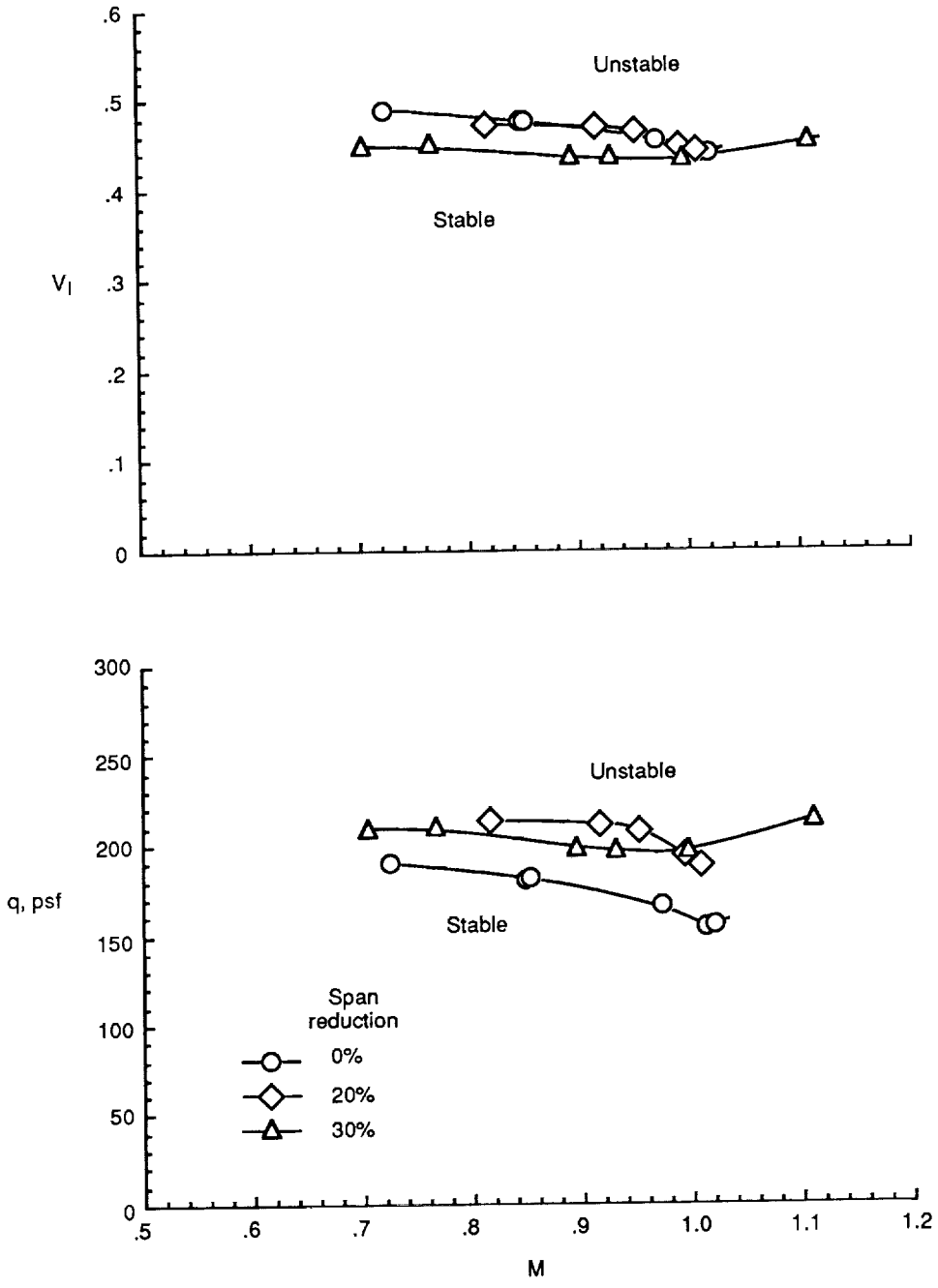

Figure 22. Experimental flutter results for wing with vertical fin configuration.

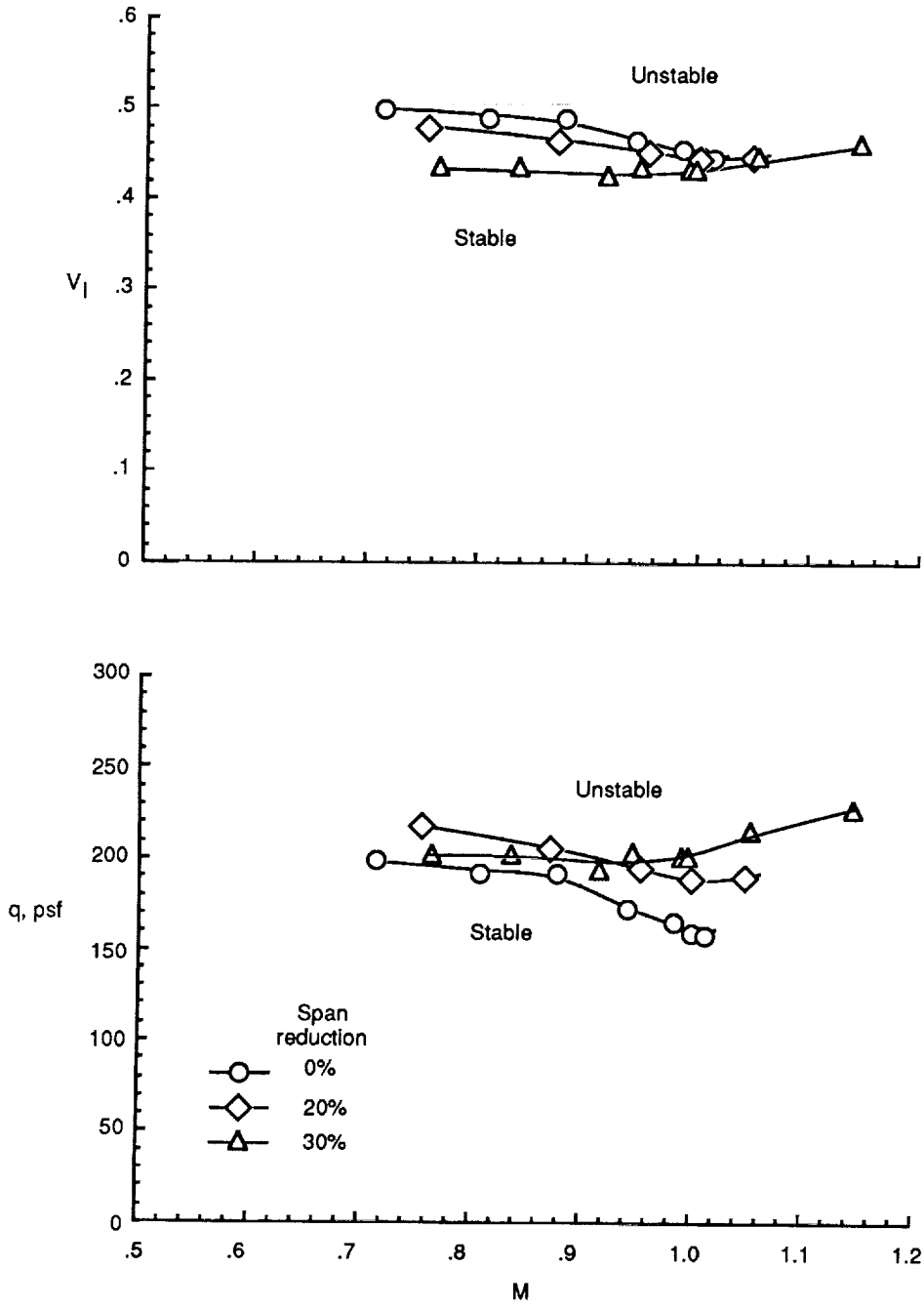

Figure 23. Experimental flutter results for wing with 45° canted fin configuration.

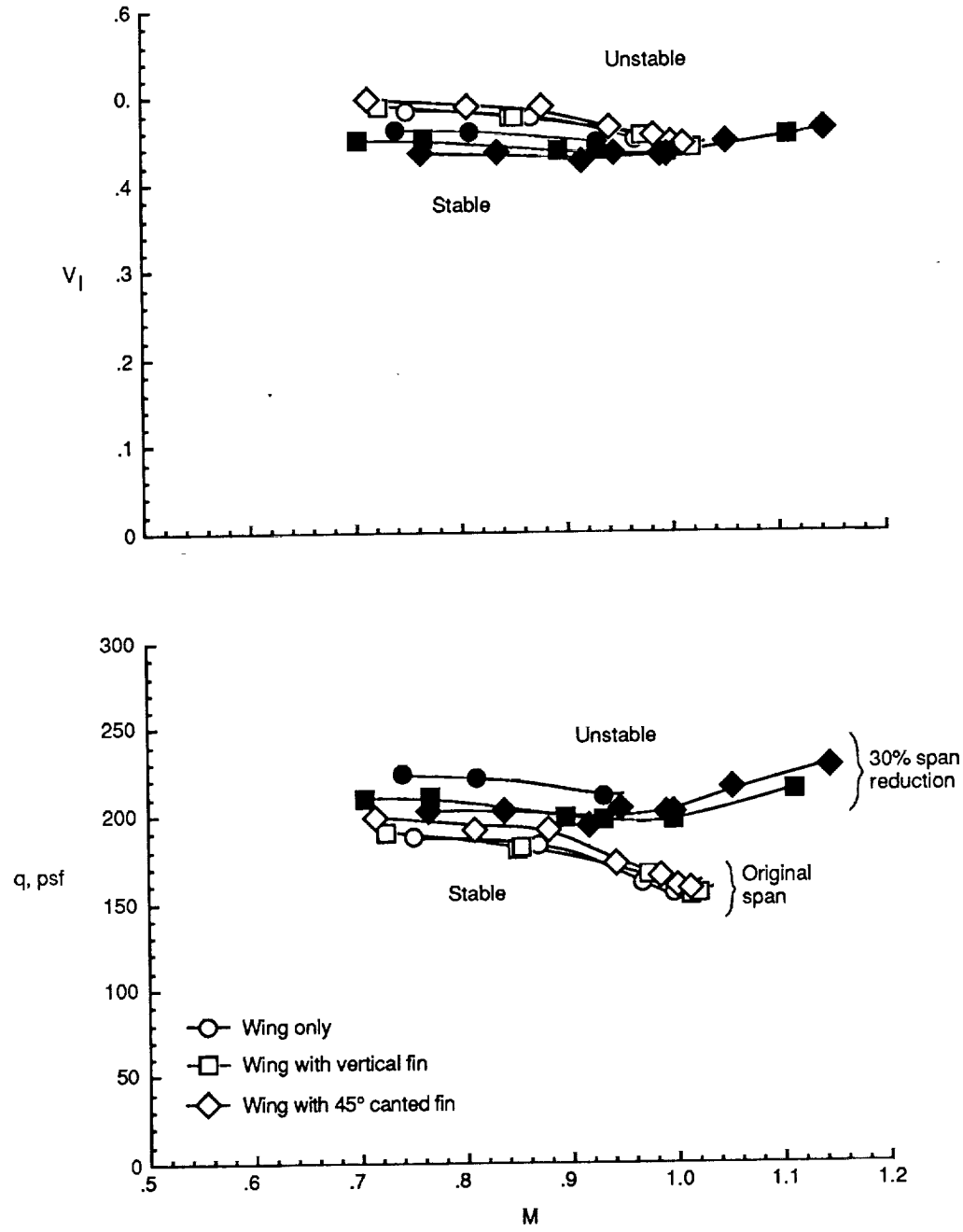

Figure 24. Experimental flutter results for wing only and wing with fin (vertical and 45° canted) configurations (original span and 30 percent span reduction).

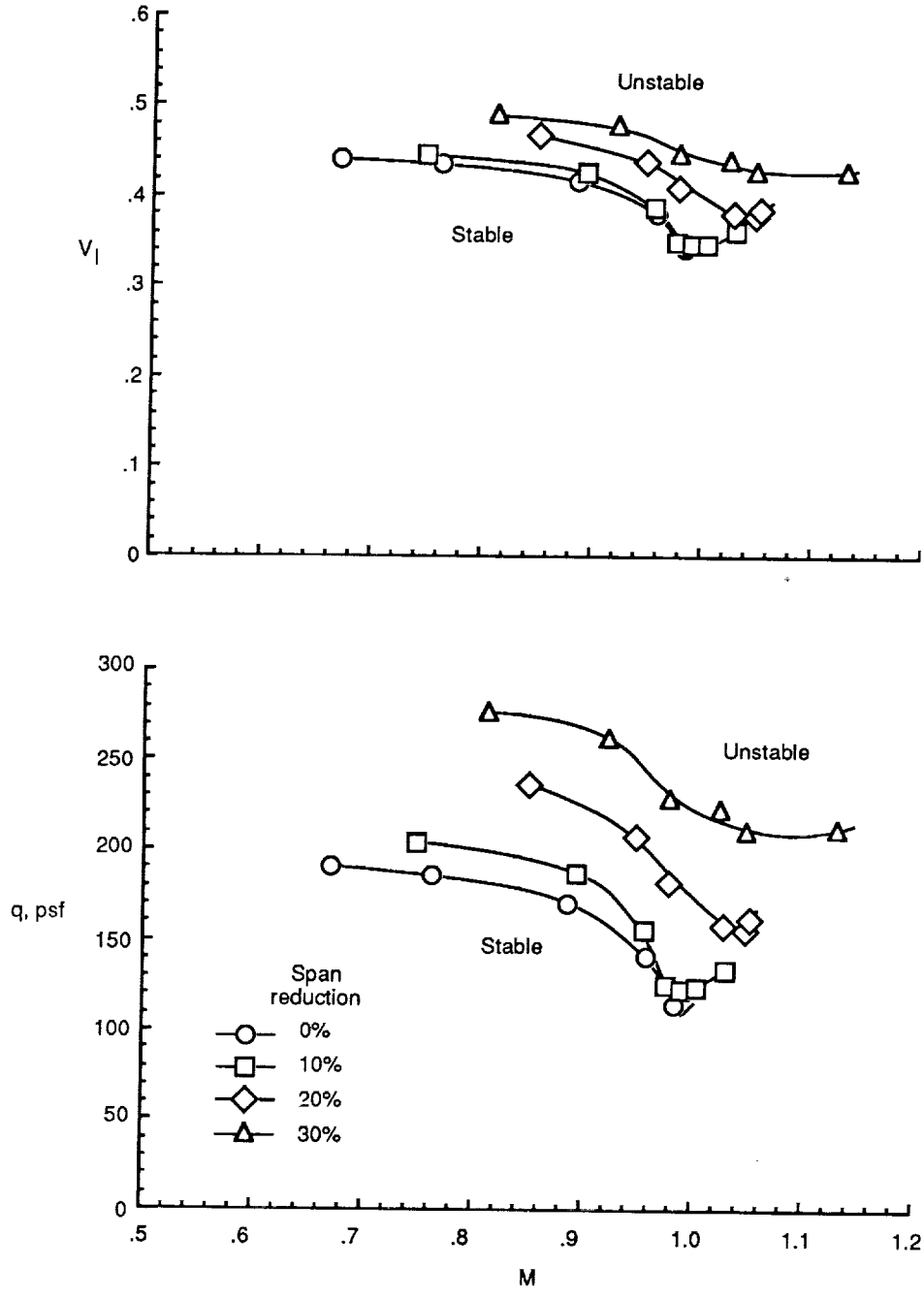

Figure 25. Experimental flutter results for wing with nacelles and vertical fin configuration.

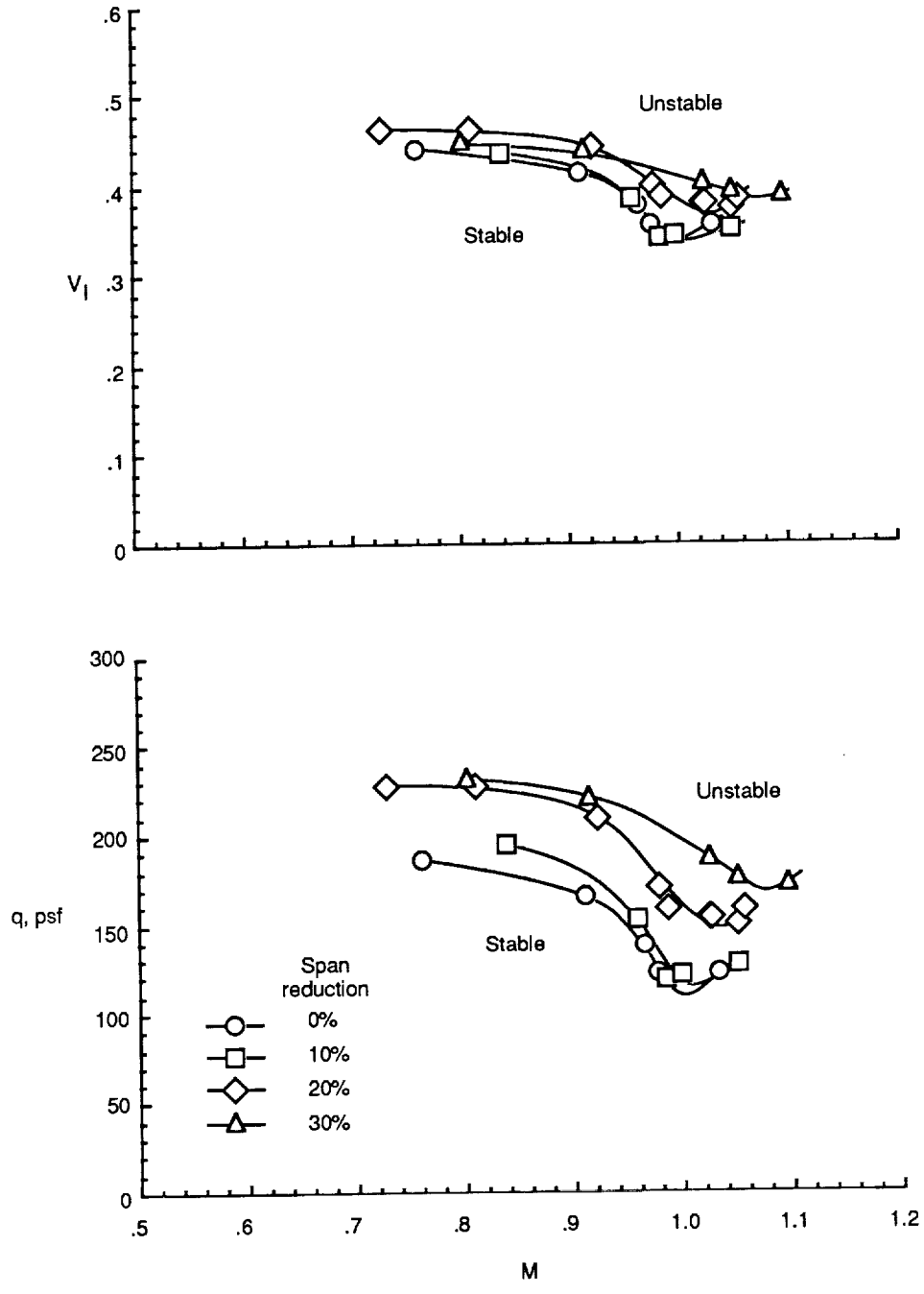

Figure 26. Experimental flutter results for wing with nacelles and 45° canted fin configuration.

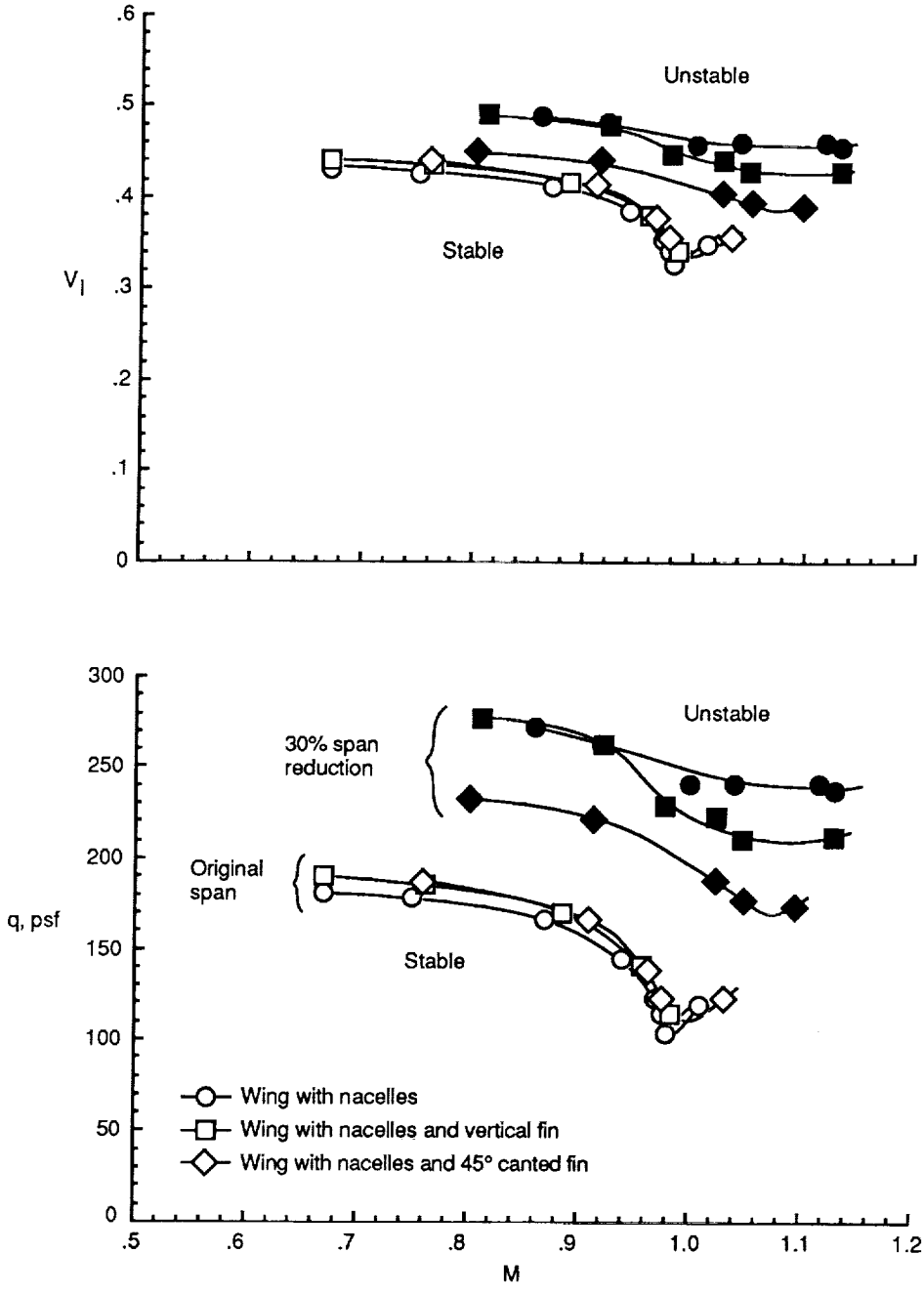

Figure 27. Experimental flutter results for wing with nacelles and wing with nacelles and fin (vertical and 45° canted) configurations (original and 30 percent span reductions).

NASA
National Aeronautics and Space Administration

Report Documentation Page

1. Report No.	2. Government Accession No.	3. Recipient's Catalog No.
NASA TP-3077		

4. Title and Subtitle	5. Report Date
Span Reduction Effects on Flutter Characteristics of Arrow-Wing Supersonic Transport Configurations	May 1991
	6. Performing Organization Code
7. Author(s)	8. Performing Organization Report No.
Donald F. Keller and Ellen Parker Bullock	L-16807
9. Performing Organization Name and Address	10. Work Unit No.
NASA Langley Research Center Hampton, VA 23665-5225	505-63-21
	11. Contract or Grant No.
12. Sponsoring Agency Name and Address	13. Type of Report and Period Covered
National Aeronautics and Space Administration Washington, DC 20546-0001	Technical Paper
	14. Sponsoring Agency Code

15. Supplementary Notes

16. Abstract

An experimental and analytical investigation was initiated to determine the effects of span reduction on the flutter characteristics of several arrow-wing supersonic transport (SST) configurations. The model was a semispan wing with the experimental flutter results obtained in the Langley Transonic Dynamics Tunnel over a Mach number range from 0.60 to 1.20. Two flow-through nacelles were used to represent wing-mounted engines. A wing fin was mounted either vertically or canted outboard at 45°. Portions of the wingtip were removed in increments parallel to the root chord to provide reductions in wing span of 10, 20, and 30 percent. Reducing the wing span increased the flutter dynamic pressure for all configurations tested. The largest increases in the flutter dynamic pressure were observed for the configurations with nacelles. Although reducing the span had little effect on flutter-speed index for the wing only and the wing with fin configurations, an increase was observed for the configurations with nacelles, particularly in the high transonic region. The flutter analysis, which generally showed the same trends as the experimental results, was consistently more conservative in the low transonic region than in the high transonic region.

17. Key Words (Suggested by Author(s))
Aeroelasticity
Flutter
Arrow wing
High-speed civil transport
Supersonic transport
Transonic
Span reduction effects

18. Distribution Statement
Unclassified—Unlimited

Subject Category 05

19. Security Classif. (of this report)	20. Security Classif. (of this page)	21. No. of Pages	22. Price
Unclassified	Unclassified	53	A04